



UNIVERSIDADE DA BEIRA INTERIOR
Engenharia

Pulsejet Engine Performance Estimation

(Versão Revista Após Discussão)

Andreia Sofia Moura Melo

Dissertação para obtenção do Grau de Mestre em
Engenharia Aeronáutica
(Ciclo de estudos integrado)

Orientador: Prof. Doutor Francisco Miguel Ribeiro Proença Brójo

Covilhã, março de 2019

Dedication

To my beloved parents and my grandparents.

*“Try not to become a person of success,
but rather try to become a person of value.”*

Albert Einstein

Acknowledgements

To my family, who always supported me unconditionally through all these years, especially my parents and my grandmother. They are the reason I came so far.

I would like to thank my supervisor, Professor Francisco Brójo, for all the help and guidance.

A big thank you to my boyfriend Pedro Pereira, for believing in me and giving me motivation during the most stressful times.

I also want to thank all my friends from my hometown and those made in my academic life, especially Sara and Inês. They are a very important part of academic life and I will take them in my heart for the rest of my life.

Last but not least, a big thank to my dear friend Diogo Moura, for reviewing this document, but above all, for being a good friend.

Resumo

Os motores *pulsejet* ganharam recentemente um novo interesse devido à sua simplicidade e possíveis aplicações em UAVs. Apesar de este tipo de motor apresentar muitas vantagens em relação a motores mais convencionais, tem diversos problemas de aplicação, nomeadamente na aviação civil, devido ao facto de ser um motor que produz muito ruído. Embora seja um motor com uma construção bastante simples, o seu funcionamento ainda não é perfeitamente compreendido, pelo que continuam a ser elaborados estudos de forma a melhorar o conhecimento relativamente à física envolta na sua operação. Este trabalho consiste numa aproximação numérica do funcionamento de um motor *pulsejet* sem válvulas. O objetivo é numa primeira fase proceder ao dimensionamento de um motor sem válvulas e, posteriormente, fazer a análise do seu desempenho para dois combustíveis assim como para diferentes caudais mássicos de combustível. Para elaborar o dimensionamento, foi feita uma rotina de cálculo baseada em dados de motores existentes e em equações referidas na literatura. O desenho do motor foi feito usando o software *CATIA V5*; a malha numérica foi criada no *ANSYS Meshing*; e, por fim, a análise foi feita no software *ANSYS Fluent 16.2*. Foi realizada uma simulação transiente em 2D. O modelo viscoso escolhido foi o *Realizable $k - \epsilon$* ; para as espécies foi escolhido o modelo de combustão sem pré-mistura (*non-premixed model*); e para o modelo de radiação foi selecionado o P1. Em relação às condições de fronteira, a entrada foi definida com base na pressão tal como a saída, a entrada de combustível foi então definida com base em três caudais mássicos: 0.04 kg/s, 0.06 kg/s e 0.1 kg/s. Foram usados dois combustíveis diferentes: propano e metano, de forma a avaliar se as diferenças apresentadas para os diferentes caudais mássicos de combustível eram comuns a ambos. Para o propano um caso adicional foi definido, sendo o caudal mássico de combustível de 0.12 kg/s. Diferentes variáveis foram analisadas para os sete diferentes casos: pressão, temperatura, frequência, velocidade, tração e a formação de poluentes. Os resultados obtidos são similares para os dois combustíveis, as variáveis apresentam o mesmo comportamento com a variação do caudal de combustível, à exceção da frequência de funcionamento. Quando é usado o metano, a frequência aumenta com o aumento do caudal de combustível, no entanto, para o caso do propano o mesmo não se verifica. Relativamente ao dimensionamento, este foi elaborado em função de uma tração desejada de 6 kg, todavia, a tração máxima obtida foi de 2.5 kg.

Palavras-chave

Pulsejet; pulsejet sem válvulas; dimensionamento; propano; metano; caudal mássico de combustível; *ANSYS Fluent*

Abstract

Pulsejet engines have recently come into the spotlight due to its simplicity and its possible application in UAVs. Even though this type of engine has many advantages over the conventional types, it still has many problems for its application, as in civil aviation due to its extreme noise. Although having a very simple construction, its operation is not completely understood, so studies continue to be made in order to have a better knowledge of the physics behind its operation. This work investigates a valveless pulsejet operation in a numerical approach. The objective includes a sizing of a valveless pulsejet and analyse the pulsejet performance with two different fuels and for different fuel mass flows. For the sizing it was done a calculation procedure based on data of existing engines and equation reported in the literature. The pulsejet was designed using the software CATIA V5; numerical mesh was created in ANSYS Meshing; and the analysis in ANSYS Fluent 16.2. It was performed a 2D transient simulation. The viscous model is Realizable $k - \varepsilon$, for species non-premixed combustion model was selected and radiation model is P1. Inlet was defined as a pressure inlet and outlet as a pressure outlet, fuel inlet was defined as mass flow inlet with three different fuel flow to be analysed: 0.04 kg/s, 0.06 kg/s and 0.1 kg/s. Two fuel where used: propane and methane, in order to evaluate whether the differences reported for the different fuel mass flow were also observed with other fuels. For propane an additional case was defined, being the fuel mass flow of 0.12 kg/s. Diverse variables were computed for the seven cases: pressure, temperature, frequency, velocity, thrust and formation of pollutants. The results obtained are similiter for the two fuels, the variables have the same behaviour with the variation of the fuel flow except for the operating frequency. For methane the frequency increases with increasing fuel flow, for propane, however, this is not verified. In the relation to the sizing, this was elaborated as a function of the desire thrust of 6 kg, nevertheless the maximum thrust obtained was of 2.5 kg.

Keyword

Pulsejet; Valveless pulsejet; sizing; propane; methane; fuel mass flow; ANSYS Fluent

Contents

1 Introduction	1
1.1 Motivation and goals	1
1.2 Document structure	2
1.3 Historical background	3
1.4 Related work	6
2 Theoretical background	9
2.1 Types of pulsejet engine	9
2.1.1 Valved pulsejet	9
2.1.2 Valveless pulsejet	10
2.2 Advantages and limitation of pulsejet	11
2.2.1 Valved vs Valveless pulsejet	12
2.3 Thermodynamic cycle	12
2.4 Kadenacy Effect	15
2.5 Acoustic Theory	15
2.6 Pulsejet frequency	16
2.7 Pulsejet components	18
2.8 Valveless pulsejet design	19
3 Numerical Modelling	21
3.1 Governing equations	21
3.2 Models	23
3.2.1 Turbulence model	23
3.2.2 Species model	24
3.2.3 NO_x formation	25
3.2.4 Radiation	26
3.3 Near wall treatment	27
4 Methodology	29
4.1 Sizing procedure	29
4.1.1 Initial sizing	33

4.2	Generation of numerical mesh.....	34
4.3	Problem setup	35
4.3.1	Boundary conditions	35
4.4	Solution	36
4.4.1	Solution methods	36
4.4.2	Solution controls	38
4.4.3	Monitors	39
4.4.4	Solution initialization and calculation set-up.....	39
4.5	Thrust calculation.....	40
5	Results.....	43
5.1	y^+ analysis	43
5.2	Propane	44
5.3	Methane.....	48
5.4	Emissions analysis	51
5.4.1	Carbon monoxide	51
5.4.2	Carbon dioxide	52
5.4.3	Nitrogen oxides.....	53
5.5	Combustion chamber pressure vs thrust	54
5.6	Frequency	56
6	Conclusion and future work	59
6.1	Conclusion	59
6.2	Future work	60
	Bibliography	62
	Appendix A.....	66
	Appendix B.....	68
	Appendix C.....	70
	Appendix D.....	72

Figures List

Figure 1 - Marconnet's pulsejet engine.....	3
Figure 2 - Schmidt Argus V1 pulsejet engine.....	3
Figure 3 - Escopette pulsejet engine.....	4
Figure 4 - Lockwood Hiller pulsejet engine.....	5
Figure 5 - Boeing pulse ejector thrust augmenter.....	6
Figure 6 - Valveless pulsejet operation principle.....	10
Figure 7 - Lenoir thermodynamic cycle.....	12
Figure 8 - Humphrey thermodynamic cycle.....	15
Figure 9 - Representation of a thrust augmentor.....	19
Figure 10 - Schubert in-line pulsejet.....	20
Figure 11 - Chinese CS pulsejet.....	20
Figure 12 - U-shaped pulsejet.....	20
Figure 13 - Non-premixed combustion.....	24
Figure 14 - Near wall treatment.....	28
Figure 15 - Pulsejet combustion chamber design.....	32
Figure 16 - Pulsejet isometric view.....	34
Figure 17 - Initial pressure distribution.....	40
Figure 18 - y^+ variation during a cycle.....	44
Figure 19 - Temperature contour for case A.....	45
Figure 20 - Temperature contour for case B.....	45
Figure 21 - Temperature contour for case C.....	47
Figure 22 - Temperature contour for case D.....	47
Figure 23 - Temperature contour for case E.....	49
Figure 24 - Temperature contour for case F.....	49
Figure 25 - Temperature contour for case G.....	50
Figure 26 - Contours of CO concentration for case G.....	51
Figure 27 - Contours of CO ₂ concentration for case G.....	52
Figure 28 - Contours of NO _x concentration for case G.....	53
Figure 29 - Combustion chamber pressure vs thrust for case C.....	54
Figure 30 - Combustion chamber pressure vs thrust for case D.....	55
Figure 31 - Combustion chamber pressure vs thrust for case E.....	55
Figure 32 - Combustion chamber pressure vs thrust for case F.....	56
Figure 33 - Combustion chamber pressure vs thrust for case G.....	56
Figure 34 - Computational vs calculated frequency for propane.....	57
Figure 35 - Computational vs calculated frequency for methane.....	57
Figure 36 - Pulsejet views a) front view, b) top view and c) side view.....	66

Figure 37 - a) Mesh overview b) approximate view of the inflation layer	68
Figure 38 - Air mass flow rate for propane.....	72
Figure 39 - Air mass flow rate for methane.	72

Table List

Table 1 - Pulsejet thrust and combustion chamber volume.....	29
Table 2 - Pulsejet engines parameters.....	30
Table 3 - Pulsejet mean areas and diameters.	31
Table 4 - Pulsejet engine lengths.	31
Table 5 - Diameter ratio.....	32
Table 6 - Pulsejet dimensions.	33
Table 7 - Mesh independence study.	35
Table 8 - Under-relaxion factors.	38
Table 9 - Obtained results for case A.	45
Table 10 - Obtained results for case B.	46
Table 11 - Obtained results for case C.	47
Table 12 - Obtained results for case D.	48
Table 13 - Obtained results for case E.	49
Table 14 - Obtained results for case F.	50
Table 15 - Obtained results for case G.....	50
Table 16 - Results of CO formation per cycle.....	52
Table 17 - Results of CO ₂ formation per cycle.....	53
Table 18 - Results of NO _x formation per cycle.....	53

List of Acronyms

CFD	Computational Fluid Dynamics
CPU	Central Process Unit
NASA	National Aeronautics and Space Administration
PDE	Pulse Detonation Engine
PDF	Probability Density Function
PETA	Pulse Ejector Thrust Augmenter
PISO	Pressure-Implicit with Splitting of Operators
UAV	Unmanned Aerial Vehicles
USAAF	United States Army Air Force
VTOL	Vertical Take-Off and Landing

Nomenclature

a	Absorption coefficient	[-]
A	Cross-section area	[m^2]
A_m	Mean area	[m^2]
c	Speed of sound	[m/s]
C_p	Heat capacity at constant pressure	[-]
C_v	Heat capacity at constant volume	[-]
D	Diameter	[m]
D_m	Mean diameter	[m]
E	Energy	[J]
f	Frequency	[Hz]
F	Thrust	[kg]
G	Incident radiation	[-]
H	Height	[m]
k	Turbulence kinetic energy	[m^2/s^2]
L	Length	[m]
m	Mass	[kg]
\dot{m}	Mass flow	[kg/s]
p	Pressure	[Pa]
P_{abs}	Absolute pressure	[Pa]
P_{gauge}	Gauge Pressure	[Pa]
Q	Heat	[J]
q_r	Radiation flux	[W/m^2]
R	Specific gas constant	[$J/kg.K$]
S_G	User-defined radiation source	[-]
T	Temperature	[K]
U	Internal energy	[J]
v	Velocity	[m/s]
V	Volume	[m^3]
W	Work	[J]
x_j	Component of the position vector	[m]

Greek letters

\vec{v}	Global velocity vector	[m/s]
μ_t	Turbulent viscosity	[m ² /s]
$\sigma_k, \sigma_\epsilon$	Constants of turbulence model	[-]
σ_s	Scattering coefficient	[-]
$\bar{\tau}$	Stress tensor	[Pa]
η	Efficiency	[-]
ρ	Density	[kg/m ³]
σ	Stefan-Boltzman constant	[W/m ² K ⁴]
γ	Heat capacity ratio	[-]
ϵ	Rate of dissipation	[m ² /s ³]
μ	Molecular viscosity	[N/(ms)]

Subscript

<i>CC</i>	Combustion chamber
<i>Cup</i>	End cup
<i>Ex</i>	Exhaust pipe
<i>In</i>	Intake pipe

Chapter 1

Introduction

1.1 Motivation and goals

Nowadays, the UAV technology is constantly improving, as this type of aircraft has created a big impact in our culture in the past years and it is expected that in a closer future the advance of this technology will bring big changes. Given this, so that might happen it is necessary to make even greater efforts, as well as to improve older technologies and find new ones.

In what concerns propulsion systems, there are many types of engines that could be used in UAVs. Depending on the type of mission for which it may be designed, many variables must be considered, and it ought to be selected a propulsion system more suitable for whichever mission the UAV is designed for. Currently the main investigation is being focused on implementing clean energy, however, the types of power sources available are not sufficiently developed yet. Electrical batteries don't have the power density needed for some specific missions and these electrical systems still need to be coupled with the conventional power sources: air-breathing systems. Older technologies are therefore still necessary, and so is the investigation about them. It is important to investigate whether they can be improved or if there will be benefits when combining them with new technologies that have been developed.

One of these technologies which isn't widely used is pulsejet engines. Major developments of pulsejet engines started in the beginning of the 20th century, but after the World War II the researches and developments of this kind of engine significantly decreased, as turbo machines took the spotlight for their applications in aviation. Recently, however, aviation has once again turned its head to pulsejet engines, as these are a great choice for UAV applications, given the fact that they have a massive advantage when compared with other engines: the simplicity of its construction. This type of engine can be made with few or no moving parts and is able to run continuously, resulting in a system which is of economical construction. Nonetheless, pulsejet engines are very noisy and produce a lot of vibration, but this does not become a constraint for its use in UAVs.

Despite being an engine with many years of history, its operation is still not completely understood. Therefore, it is necessary to study the behavior of this type of engines under different conditions. The motivation for doing this work is to study the simplicity of an old propulsion system and its performance under different variables, and posteriorly report the consequent effects in the engine operation.

Primarily, the main goal is developing a calculation routine to perform an initial sizing of the engine. Then, an CFD analysis will be taken in order to verify if the initial sizing leads to a functional engine.

An important step to take firstly is an intensive research of technical literature to gather relevant information about pulsejets. This review will be extremely helpful to understand the operation principles of this type of engine.

Secondly, for the sizing, is necessary to find the plans of existing engines and make a statistical study to determine the relation between the different parts of the engine and then obtain a draught of the design. After this, using software Ansys Fluent 16.2 an evaluation of the engine performance will be made. In addition, different parameters in performance of the engine will be evaluated for different fuels and different fuel mass flow rates.

1.2 Document structure

The first chapter is about the purpose of elaborating this master's thesis and the explaining of the motivation that led to this work. In this chapter it is also described the goals behind this investigation and what is supposed to be achieved through it. A historical review is presented in order to understand the evolution of these engines and their application through the decades. It is also included a small review of the most relevant works for this theme.

Second chapter is a theoretical background: an overview of the pulsejet operation. In this chapter is explained the physics behind its functioning.

In third chapter an introduction is made to the theory behind the numerical modelling. The governing equations are presented, and the models used in this simulation, as well as the near wall modelling, are clarified. It is also described the procedure for the thrust calculation.

Fourth chapter is the parametric study: here it is described the method used to do the sizing of the engine and the numeric model. Are explained all the process that led to the sizing and the final dimensions of the engine presented. The mesh independence study, the boundary conditions and the solution methods are included as well.

Fifth chapter contains the presentation and discussion of the results obtained. It is explained what was expected and what is new, there is also reference to possible mistakes that might have happened. The final goal is to compare these results with other reported in the literature.

In the final chapter it is presented the ultimate considerations and the conclusion that can be withdrawn with the accomplishment of this work. Proposals for future work in the field are taken in consideration.

1.3 Historical background

References to pulse combustion and its applications date back to late 17th-early 18th centuries and the contributions of Huygens and Allen are noteworthy. These references generally deal with the complex fluid-thermo-chemical processes that control the operation of various pulse combustors and oscillating flames, and pulse combustion applications. Major developments of pulse combustion applications started in the beginning of the 20th century and led to the development of the Esnault-Peltre, Holzworth and Karavodine gas turbines that utilized a pulse combustion process to burn the fuel [1].

In 1906, Russian engineer Vladimir V. Karavodin found a way to evaluate the frequency, stability and thrust produced for different diameters and lengths. A year later, based on his research, he successfully builds a working pulsejet engine which was a high velocity pulsed gas jet generated by a cyclic combustion of a liquid hydrocarbon fuel/air mixture [2].

Marconnet developed the first valveless pulsejet in 1909, although his patent was for a valved pulsejet engine (see fig. 1). His project is composed of an inlet diffuser, combustion chamber and a long outlet diffuser to direct most of the combusted mixture through exhaust pipe rather than through intake [3].

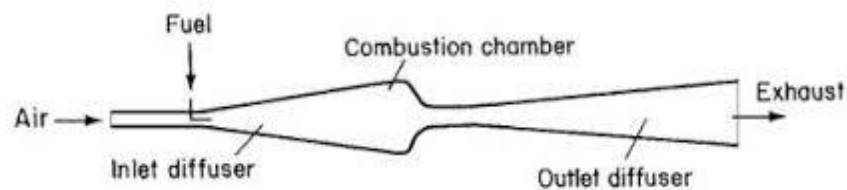


Figure 1 - Marconnet's pulsejet engine [3].

In 1931 German Paul Schmidt patented a valved pulsejet and eight years later his technology was manufactured by Argus Company. This engine, Schmidt Argus V1 pulsejet (see fig. 2), is the most famous pulsejet engine due to its use to power the *Vergeltungswaffe*, better known by V-1 flying bomb, which was extensively used in World War II.

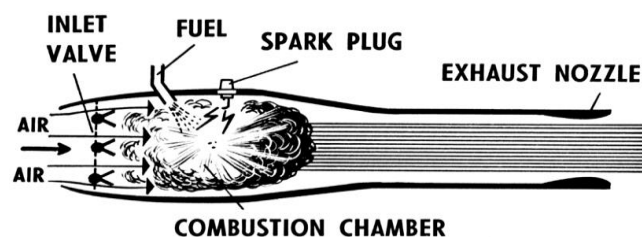


Figure 2 - Schmidt Argus V1 pulsejet engine [3].

After the World War II, the United States created Project SQUID as an effort to improve pulsejet and rocket engines, this project was run by the Office of Naval Research [4]. In 1944 USAAF (United States Army Air Force) and America industry developed Jet Bomb 2, more informally known as “Thunderbug”, whose first successful launch was on 5th June 1945. The US Navy also built its V-1 variant, the KUV-1 Loon. Many other countries also tried to make their own variant of V-1 flying bomb. During 1940s, USSR and Japan produced their derivatives and copies of the flying bomb, and in the 1950s, the French developed a target drone named “Arsenal 5.501” which was similar to the V-1 but had twin tail fins and radio control.

Lt. William Schubert of the US Navy designed his valveless pulsejet engine in the beginning of 1940s. His project had two improvements over Marconnet’s: the design of the combustion chamber and the intake geometry. The entry of the combustion chamber has abrupt change of the area which produces high turbulence and allows a better mixture of the air and fuel. For the intake, Schubert created a new geometry that allowed the exhaust gas to remain in the combustion chamber until the pressure inside falls below atmospheric [5].

In 1950, Bertin and the SNECMA Corporation developed Escopette Pulsejet (see fig. 3), this was considered the best performing engine to date. Among its improvements, we highlight the presence of a recuperator, which is a curved tube mounted at some distance from the intake. In admission of fresh air, the engine breathes through the opening between the intake and the recuperator. During the expansion, the hot gases are expelled through the exhaust pipe, although a small portion of them are expelled through the intake. In this phase of the combustion cycle the recuperator acts as a part of the engine turning the hot flow backwards and increasing the thrust. The flow, in the intake phase, is negatively affected by the presence of the recuperator, however, its presence compensates in exhaustion phase by reducing the effective length of the engine and so improving the efficiency of the engine. Another improvement is in the exhaust pipe which until now was a straight pipe, in this model it is, however, divided to increase the area of the section. As can be seen in the figure below, the engine exhaust pipe is composed by two straight and two conical sections and the transition point between the different sections causes a reflection of the pressure waves. After this reflection the pressure wave turns as a rarefaction wave, which can be considered a negative pressure wave, and this phenomenon will improve the vacuum formed in the combustion chamber, thus increasing the aspiration of fresh air during the intake phase [3] [6].

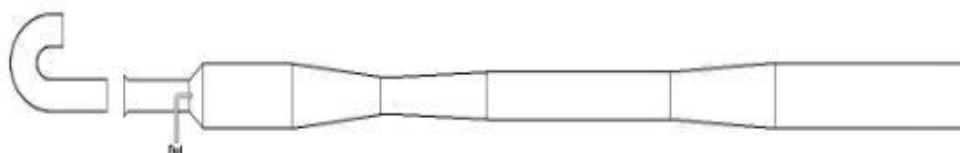


Figure 3 - Escopette pulsejet engine [3].

In the following years, interest in pulsejet technology strongly decreased, as developments in turbojets brought more attention, even so some research continued to be done concerning pulsejet engines.

Between 1950 and 1960 the Lockwood Hiller engine appeared (see fig. 4), a U-shaped valveless pulsejet. This engine can be seen as the successor of the Ecrevisse engine, developed by SNECMA, and may be also considered the most effective pulsejet in history. One particularity of this engine is the fact that it does not have any straight part, the section area changes constantly. This non-uniform cross section brought some improvements when compared to the engines developed so far. Among such improvements are “easier engine starting, greater permissible range of variation in the rate of fuel delivery accommodated by the engine, and higher ratio of thrust and air-handling capacity of the engine per unit volume thereof” [7].

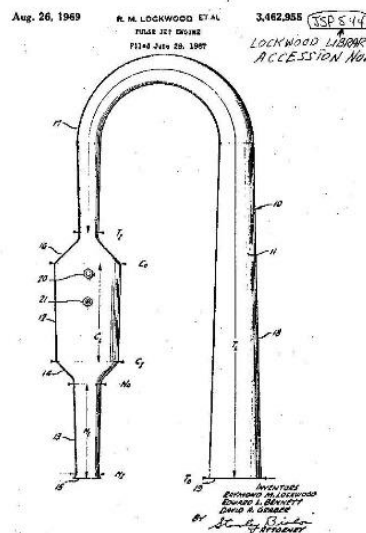


Figure 4 - Lockwood Hiller pulsejet engine [7].

Another pulsejet model is the Thermojet, that is a valveless pulsejet designed by John A. Melenric [3]. The design of this is very similar to other ones that appeared at that time except that this one had two (could even had four) intakes parallel to the tailpipe, allowing the intakes to be shorter.

More recently, Boeing patented a Pulse Ejector Thrust Augmenter (PETA) - see Fig. 5, through which proposes the use of valveless pulsejet engines for vertical take-off and landing aircraft (VTOL). Each pulsejet includes a combustion chamber having an upstream inlet port joined to an inlet diffuser, and a downstream exit port joined to a discharge nozzle. Each pulsejet discharges into an ejector to increase net thrust. Each ejector includes an augmentor cell. This design was patented in the beginning of the 21st century, however, to the date no major developments have been done [8].

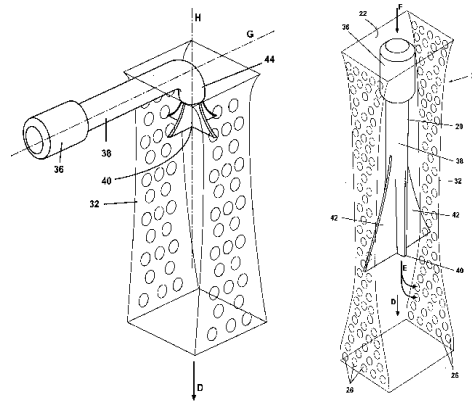


Figure 5 - Boeing pulse ejector thrust augmenter [8].

In the last years pulsejet engines earned a new interest, particularly for its use in UAV propulsion. The main researches have focused on PDE (pulse detonation engines): PDE works on detonation of the fuel air mixture (this is a supersonic combustion), while conventional propulsion engines use deflagration, which is a subsonic combustion. Although this type of engine is attractive for its structural simplicity, its operation is not that simple. The high noise levels remain a problem that have not been overcome and are the main impediment of their use.

1.4 Related work

The majority of the studies undertaken more recently are focused in valved pulsejet engines. The attractiveness behind pulsejet engines depends upon the fact that they are very easy to build on small scales. They can be constructed into low-cost micro-scale propulsion devices for use in many new applications such as UAVs. However, attempts to design and build a valved 15 cm pulsejet were unsuccessful due to the reed valves, so traditional valved inlet was replaced with a valveless inlet [9]. The smallest valveless pulsejet reported is by Geng et. al. and has 8 cm [10].

In terms of sizing, there is no calculation routine found in literature, although there are studies that present guidelines on how to do a proper sizing. Based on observations, the exhaust tube internal diameter should be half the maximum combustion chamber's internal diameter. And, the internal diameter of the intake tube should be around three fourth of the exhaust's internal diameter. Kudesia and Bisen also state that valveless pulsejet are highly dependent on the way the fuel is delivered and on the location of the fuel stream [11]. It is important to have an appropriate sizing of pulsejet's components, since it will influence its operation.

A report of a 50 cm valveless pulsejet shown that with increasing intake tube diameter both frequency and exhaust temperature at outlet increased, while inlet temperature decreases [2].

The lengths of intake and exhaust tubes are also important, the operation frequency increases with decreasing exhaust tube length or with increasing intake tube length [9] [2]. In the study of 8 cm valveless pulsejet some conclusions relatively to the fuel mass flow rate are stated. For rearward-facing inlet, the operation frequency and peak pressure increases with increasing fuel mass flow. Also, there have been comparisons between the thrust produced in a forward and rearward-facing inlet. As expected, less thrust was measured in the configuration with a forward-facing inlet [10].

Chapter 2

Theoretical background

2.1 Types of pulsejet engine

Pulsejet is the simplest type of jet engine, it can be made with few or no moving parts and can run statically. It is basically constituted by cylindrical and hollow sections. Its simplicity makes engines easy to manufacture and cheap to produce. The intake of air is intermittent, and this results in a pulsating combustion. A pulsating combustion is a burning process through acoustic oscillations: the fuel and air are submitted to compression and decompression rising the mixture efficiency and consequently the combustion reaction.

Based on the valves, there are two types of pulsejet engines:

- Valved pulsejet;
- Valveless pulsejet.

2.1.1 Valved pulsejet

The valved type has a set of one-way valves that controls the admission of fresh air through the intake. To start the engine, it is necessary the admission of compressed air, for which the valves must be open. If the pulsejet is stagnant and there is no relative air velocity it is necessary to provide compressed air by an external equipment, but if it is moving the air dynamics pressure provides the necessary air compression. The fuel can be mixed with air directly in the intake or it can be injected into the combustion chamber (it is either a gas or liquid aerosol) and, after the mixture, the ignition is made using a spark plug. When the combustion occurs the pressure inside the combustion chamber increases shutting the valves. With the valves closed, the combustion gases have only one way to be expelled: through the exhaust pipe, producing forward thrust. Due to inertia of the exhaust gases, the pressure in the combustion chamber strongly decreases, allowing the valves to open again and admit a new portion of fresh air and a new cycle begins. In this new cycle the use of a spark plug to start ignition is not necessary, as the mixture is ignited by the residual heat from the previous cycle. The cycle frequency of valved pulsejet depends mainly on the length of the engine: the smaller it is, the bigger the frequency [12].

2.1.2 Valveless pulsejet

Valvess pulsejet is the simplest type of engine, there is no moving parts and both admission and exhaust are controlled by its geometry. It can also be designated as aerodynamic valved pulsejet, acoustic-type pulsejet or intermittent ramjet [5]. This type of pulsejet usually has the intake and the exhaust pipe in the same direction. As in the valved pulsejet the cycle begins with the intake of compressed air and fuel. To start the engine the use of a spark plug is necessary to ignite the fuel air mixture. Once the engines start, the spark plug become unnecessary since the residual heat in the combustion chamber ignites the mixture, as it happens in valved engine. The combustion increases the temperature and pressure in combustion chamber, causing the gases to expand and causing a compression wave which travels through the intake and exhaust pipe. The pressure wave reaches the end of the intake pipe first and then it is reflected in the opposite direction as a rarefaction wave. Although this rarefaction wave is weak it can reserve the gases and admit fresh air into the intake pipe. When the compression wave reaches the end of the exhaust pipe, it is also reflected as a rarefaction wave, this one takes more time to happen because the exhaust pipe is longer. Rarefaction wave travels back to the combustion chamber but, due to inertia, the hot gases continue to be expelled through the exhaust pipe. The momentum of the gas pulse assists the hot gases reversing direction. When the rarefaction wave arrives in the combustion chamber the pressure falls below the atmospheric and this permits the intake of fresh air. At this point the exhaust gas continues flowing out through the exhaust pipe and the rarefaction wave is reflected from the end of the combustion chamber. After this reflection the flow in the exhaust pipe start to reverse and the rarefaction wave is reflected again and turns back to the combustion chamber as a compression wave. At this point, the admission of fresh air is slowed down allowing the combustion to start and the cycle repeats. It is important to notice that, inside the pulsejet, the wave travels at the speed of sound, though due to the temperature this speed is higher that it would be in normal conditions [13].

The movements of the gases may be explained by the Kedenacy Effect and the Acoustic Theory and both will be clarified further ahead (see Fig. 6).

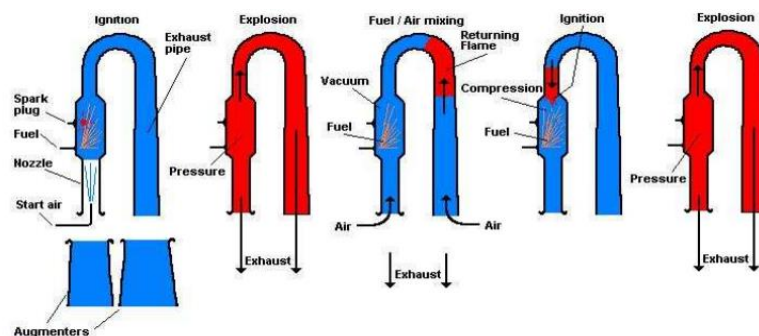


Figure 6 - Valveless pulsejet operation principle [33].

2.2 Advantages and limitation of pulsejet

The first thing about pulsejet engine that excited the researchers was its self-sustaining operation, which is a peculiar pulsating combustion propriety. The combustion is intermittent and does not occur at a constant pressure such as in most of jet propulsion systems. The succession of explosive pulses causes a pressure increase inside the combustion.

Pulsejet is the only jet engine that shows a net pressure gain between the intake and the exhaust. The exhaust pressure is higher than the intake pressure and this happens without wasting the power generated by combustion. This pressure gain, which is about 5%, improves the overall efficiency, however, it is difficult to use this gain for propulsion. A way to improve the potential of pulsejet engine is to use them as a combustor for a turbine engine, because its pressure gain will be multiplied in a high-pressure environment [14].

These engines can be made in different sizes with different thrust outputs, which is an economical advantage in the field of miniature propulsion. It has a very high thrust-to-weight ratio.

A major advantage is its simplicity: it has been already mentioned that pulsejet have little or no moving parts, which makes it easy to maintain and cheap to produce. It has also a great heat capacity, it uses atmospheric oxygen and cheap fuels. They can run statically and do not need to have air forced into the inlet by forward motion. If compared with traditional constant pressure combustors, pulsejet have smaller mechanical losses [14].

Studies have proved that when compared with normal combustion (without pulsating effect) pulsed combustion revealed to be more efficient: the amount of unburned gases leaving the combustion is less in pulse combustion. Due to its extremely efficient combustion, these engines do produce less dangerous pollutants, even when using hydrocarbon fuels [15].

Nonetheless, pulsejet engines still have some disadvantages which make them less attractive. They have low compression ratio, low specific impulse, very low thermodynamic efficiency, high rates of fuel consumption and reliability. A consequence of their pulsation combustion is the production of high noise levels and vibration, making its use in civil aviation impossible.

Its speed is limited to a very narrow range between 650-800km/h. This limitation is due to the difficulty of creating an aerodynamic efficient intake suitable for a wide speed range. The operational altitude is also limited [16].

The weighing of these advantages and disadvantages makes pulsejets a great choice for its application on some UAVs missions.

2.2.1 Valved vs Valveless pulsejet

Valved pulsejet engine is a very simple engine with the valves being the only moving part, nonetheless, researchers wanted to make it even simpler and so removed the valves. This little change brought some advantages and disadvantages.

The major problem of valved pulsejet is the short lifetime of the valves, as they limit the engine operating life. Besides that, the use of valves makes the construction more complex and expensive. Depending on the type of the valves used, they are limited to a maximum thrust. The smaller pulsejet engine use petal valves system, which has a very short lifetime. Tests developed by NASA in 1948 verified that when subjected to extreme temperatures, pressures and frequencies these valves last approximately fifty seconds [17].

Valveless engine solved the major problem as the absence of valves extended the engine's operating life, though diminishing the efficiency and performance, causing also the production of more drag.

2.3 Thermodynamic cycle

To a better understanding of the operation principle of pulsejet engines it is important to know the thermodynamics involved. Some authors consider that the operation of a pulsejet engine can be described by the combination of two thermodynamics cycles: Lenoir Cycle and Humphrey Cycle [18]. However, other authors affirm that the Lenoir Cycle explains the working of a pulsejet engine and the Humphrey Cycle describes the operation of pulse detonation engine.

The Lenoir cycle is based on the operation of an engine fabricated in 1860 by the Belgian engineer Jean Joseph Étienne Lenoir (see Fig. 7). The ideal cycle consists of a constant volume heat addition, followed by an isentropic expansion, and finally a constant pressure heat rejection.

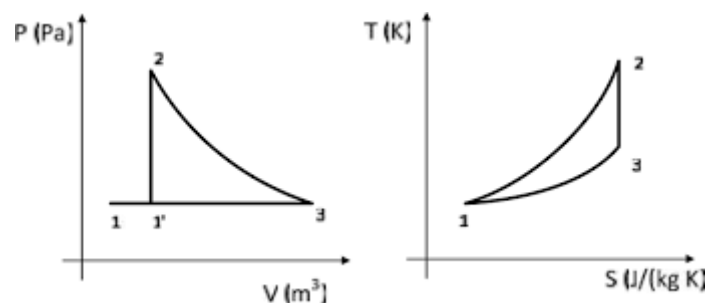


Figure 7 - Lenoir thermodynamic cycle [14].

- Constant volume heat addition (1-2)

The first stage of the ideal cycle involves the combustion in a constant volume process, this leads through the first law of thermodynamics:

$$Q_{1-2} = mc_v(T_2 - T_1) \quad (2.1)$$

$$c_v = \frac{R}{\gamma - 1} \quad (2.2)$$

As the volume is constant, there is no work involved:

$$W_{1-2} = \int_1^2 p dV = 0 \quad (2.3)$$

The pressure after the heat addition can be calculated from the ideal gas law:

$$p_2 V_2 = RT_2 \quad (2.4)$$

- Isentropic expansion (2-3)

This stage involves a reversible adiabatic expansion of the fluid back to the original pressure. An isentropic expansion can be expressed in function of temperature, pressure and volume.

$$\frac{T_2}{T_3} = \left(\frac{p_2}{p_3}\right)^{\frac{\gamma-1}{\gamma}} = \left(\frac{V_3}{V_2}\right)^{\gamma-1} \quad (2.5)$$

In this specific cycle can be affirmed that $p_3 = p_1$, and as this stage is an adiabatic expansion $Q_2 - Q_3 = 0$, so the first law of thermodynamics can be written as:

$$W_{2-3} = \int_2^3 p dV = p_2(V_3 - V_2) \quad (2.6)$$

- Constant pressure heat rejection (3-1)

The final stage involves a constant pressure heat rejection, the first law of thermodynamics and the definition of work can be described by:

$$Q_{3-1} - W_{3-1} = U_1 - U_3 \quad (2.7)$$

$$W_{3-1} = \int_3^1 p dV = p_1(V_1 - V_3) \quad (2.8)$$

The amount of heat rejected is given by the following equation:

$$Q_{3-1} = mc_p(T_3 - T_1) \quad (2.9)$$

$$c_p = \frac{\gamma R}{\gamma - 1} \quad (2.10)$$

The overall efficiency can be determined by:

$$\eta = \frac{W_{2-3} - W_{3-1}}{W_{1-2}} = \frac{\int_2^3 p dV + p_1(V_1 - V_3)}{mc_v(T_2 - T_1)} \quad (2.11)$$

It ought to be mentioned that pulsejet engine gains work during the expansion phase, though some is lost during the heat rejection phase.

The Humphrey cycle is very similar, adding only a small compression before the combustion. This cycle involves an isentropic compression, constant-volume heat addition, isentropic expansion and a constant-pressure heat rejection (see Fig. 8).

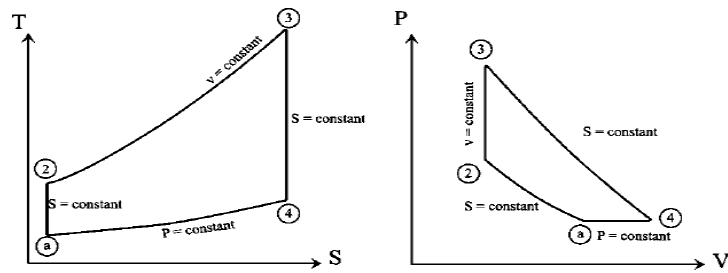


Figure 8 - Humphrey thermodynamic cycle [5].

2.4 Kadenacy Effect

The Kadenacy Effect was first discovered in 1600s by Christiaan Huygens, a Dutch physical scientist, although its name comes from the physicist Michael Kadenacy, who developed an engine in 1933 which operates according to this effect. It explains that when high pressure air leaves a vessel quickly through a large opening, the pressure inside the vessel drops to ambient pressure. Due to the inertia of the gases the air continues to flow out, causing the pressure inside to drop below the atmospheric. The difference of pressures stops the outflow and allows the intake of fresh air into the vessel [19].

In pulsejet engines, the combustion is responsible for increasing the temperature and pressure in the combustion chamber, and this leads the hot gases to flow out. The momentum of the gases leaving the chamber causes the pressure-drop and this allows the intake of fresh air. The inertia causes a pressure oscillation, consequently the air and the combustion gases are compressed between the inside and the outside pressures. This pressure differential originates a partial vacuum effect in the combustion chamber, because of this a fresh fuel-air mixture is led into in the combustion chamber and the gases in the exhaust pipe will be dragged back inside the engine. Thus, the pressure inside increases and the ignition of the fresh mixture occurs.

2.5 Acoustic Theory

Another explanation for the operation of pulsejet engines is the acoustic resonance theory. It ought to be noted that both acoustic theory and Kadenacy effect can explain pulsejet operation, but they differ slightly. Kadenacy effect explains pressure variation through the flow displacement, while acoustic theory explains the same through the pressure waves. The second focuses on small perturbations around the equilibrium, small pressure changes, low gas velocities and little gas displacement. In short, along the exhaust pipe occurs an exchange of momentum between small regions of the fluid.

In acoustics there is nodes and antinodes, which represent the places where velocity and pressure changes are minimal or maximum. In the combustion chamber the pressure swings are

the greatest, seesaws regularly above and below atmospheric. On other hand, the movement of gases is restricted, so it is a pressure antinode and a speed node. At the end of the intake and exhaust the speeds changes are greater and the pressure variations are minimal. Here we have speed antinodes and pressure nodes. The distance between a node and an antinode is a quarter of the wavelength. Normally in an open tube this distance is half of the wavelength, but in valveless engine it is closer to reality to assume as a quarter of the wavelength [19]. When the deflagration occurs in the combustion chamber, as explained, generates two waves fronts, one travels through intake and the other one through exhaust pipe. In acoustic terminology it can be said that conventional pulsejet engines operate on a 4L wave system, four pressure waves: compression - rarefaction - rarefaction - compression [5].

2.6 Pulsejet frequency

An important characteristic in pulsejet engines is its operation frequency. This is another variable where the authors' opinion is divided as there are different models to predict the operation frequency. However, pulsejet engines can be made in many different sizes, so these formulas are not necessarily wrong.

Following the acoustics theory, the operating frequency is primarily related to the overall length and pulsejet can be modelled as an acoustic quarter-wave tube with a pressure node at exhaust and a pressure antinode in combustion chamber [20]. According to this theory the frequency can be calculated by:

$$f = \frac{c}{4L} \quad (2.12)$$

This model was found to have a good agreement when experimenting for valved pulsejet, however, for valveless pulsejet it has not been proved so correct. Some researchers [2] showed that for a valveless pulsejet the exhaust pipe acts closer to a sixth wave tube:

$$f = \frac{c}{6L} \quad (2.13)$$

Another model is the lumped-parameter Helmholtz resonator, which treats the intake and exhaust pipe as incompressible masses and combustion chamber as a compressible volume [21]. However, recent studies proved this model as over predictive of operation frequencies [22].

$$f_{LP} = \frac{1}{2\pi} \sqrt{\gamma \frac{P}{V_{cc}} \left(\frac{A_{in}}{\rho_{in} L_{in}} + \frac{A_{ex}}{\rho_{ex} L_{ex}} \right)} \quad (2.14)$$

An important model proposed by Zheng et al. [23] considers that valveless pulsejet is a combination of a Helmholtz resonator and a long resonance-tube attached to a large volume. The combination of the intake pipe and combustion chamber can be taken as a Helmholtz resonator and its frequency is given by:

$$f_{in} = \frac{c}{2\pi} \sqrt{\frac{A_{in}}{V_{cc} L_{in}}} \quad (2.15)$$

The exhaust pipe frequency is given by the following equation:

$$\frac{2\pi f_{ex} V_{cc}}{A_{ex} c} \tan\left(\frac{2\pi f_{ex} L_{ex}}{c}\right) = 1 \quad (2.16)$$

Based on this study, the overall operation frequency of the valveless pulsejet was assumed to be the average of the intake and exhaust frequency:

$$f = \frac{f_{in} + f_{ex}}{2} \quad (2.17)$$

In the last years, many studies have been evaluating the influence of the intake and the exhaust pipe lengths on the operational frequency. Zheng et al. [23], based on their model, concluded that the operating frequency increases when the intake diameter increases and the intake and exhaust pipe length decreases. This conclusion was also supported by other studies using other models for calculating the operating frequency [13] [2]. More recently, at the University of Maryland, the operation of valveless pulsejet was analysed using a fluid-electrical analogy and transmission line theory [22]. This study compared the measured frequency in five different configurations with the calculated frequencies using three different models: Lumped Parameter, Zheng et al. and the latter method. The findings agreed with the previous conclusions, though this new model revealed more accurate results.

2.7 Pulsejet components

Pulsejet engines can be built in different designs and sizes, however there are some requirements that should be taken in account. Over the years, studies stated some conditions that must be satisfied in order to achieve the pulsating effect.

The design of a pulsejet involves seven basic components:

- To start the engine requires the use of an external equipment to supply compressed air to the engine. Once the engine is running, this is no longer necessary.
- An intake from which the air admission is made. The fuel can be drawn into the engine through an atomizer and is mixed with the air in the intake. This has the advantage of a great simplicity and requires no fuel pump or other auxiliary equipment. The intake should have the necessary dimensions, so it can fill combustion chamber with fresh air during the intake phase. A too long intake would have the same working as an exhaust pipe: at some point the exhaust gases which travel through the intake will reverse direction to the combustion chamber, filling it with residual gases instead of fresh air. A too small intake will limit the portion of fresh air to be admitted. This will result in a poor combustion, causing very few combustion gases forced into the exhaust pipe. The intake pipe should be wider at the combustion chamber end and narrower at the opening. This provides an additional choking effect during combustion and an increase in pressure which leads to a more efficient combustion.
- A combustion chamber, where deflagration of fuel-air mixture occurs. The combustion increases the pressure and forces the gases out through the exhaust pipe and, in case of valveless pulsejet, the gases are also expelled through the intake. The sizing of this part is important to have a good combustion efficiency. If the combustion chamber is too small it is possible that it won't support all the fresh air from the intake, causing the air to escape into to the exhaust pipe, and in this case, it may not be burnt. A too large combustion chamber is not a good choice either as it would reduce the vacuum effect, thus reducing the intake of fresh air making the combustion less efficient. Besides that, it will contain too much residual gases which will also affect the efficiency.
- Pulsejet engines can have or not valves. This component separates the intake and the combustion chamber, and it forces the hot gases to leave the engine only through the exhaust pipe. In intake phase, the valves open and allow the entry of fresh air, after that, they close, so the gases won't escape through the intake. For valved engines valve area is a very important parameter.
- The most common ignition source to start the engine is a spark plug. There are other options to ignite the mixture, though this is the most reliable. This device is mounted in the combustion chamber zone.

- The fuel can be delivered through aspiration or injection. In aspiration the fuel is drawn into the engine through an atomizer, in injection the fuel is sprayed directly in the combustion chamber. The second method has the advantage that the engine can be throttled by varying the amount of fuel supplied [24].
- The last component is the exhaust pipe. The major part of the gases is expelled through here. This part of the engine can have different designs as seen in the historical background. It can be a straight cylindrical pipe, or it can have sections with different diameters. In the project design the determination of exhaust pipe length is a crucial part. If it is too short, the exhaust gases will all leave the engine, therefore any residual heat will not remain to ignite the fresh mixture. Besides that, the rarefaction wave will reach the tube end too soon and will not interact optimally with the partial vacuum caused by the momentum of the exhaust gases. On the other hand, if it is excessively long, the exhaust gases will cool down too much making the ignition of the mixture difficult or even impossible. In this case the rarefaction wave will take too long to be reflected, thus its energy being loss.

In addition to these components there are others that can be added to the design to improve performance. A thrust augmentor (see Fig. 9) is a device implemented in the exhaust of the engine with the purpose of increasing thrust. This element does for the pulsejet what an afterburner does for a turbojet. The hot gases leave the engine through the exhaust pipe at a high velocity and low pressure, allowing the cold air to be sucked to the augmentor. This generates turbulence and the hot and cold air mix heating the cold air. With the increasing temperature, the gases expand and the thrust increases.

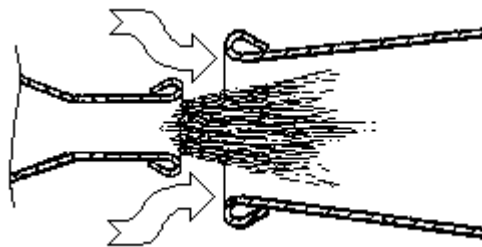


Figure 9 - Representation of a thrust augmentor [3].

As mentioned in the previous section it can also be applied a recuperator before the intake. This component will also increase the produced thrust.

2.8 Valveless pulsejet design

Over the years, different configurations for these engines came up, as seen in historical background. There are three main designs: in-line, linear and U-shape engines [25].

The in-line configuration has the intake and the exhaust pipe in the same axis, though they are in opposite directions (see Fig. 10). This design is probably the oldest and it can be recognized as the Marconnet's pulsejet. The major advantage of this model is distinguishable when the engine is moving forward: the air is pushed into the intake increasing the static pressure inside the intake - the ram-air effect. This leads to a higher mass-flow through the engine. On the other hand, having intake and exhaust pipe in different directions will decrease the total thrust, since some gases will be expelled through the intake pipe.

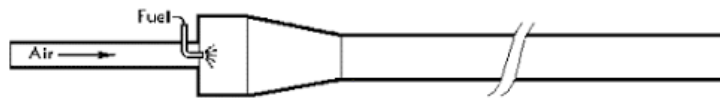


Figure 10 - Schubert in-line pulsejet [3].

Linear configuration is very similar to in-line, however here the intake and exhaust pipe are pointing in the same direction which consequently solves the problem of the previous, since the thrust generated by the intake pipe adds to the total thrust (see Fig. 11). Although improving the thrust problem, it loses the ram-air effect. The Chinese pulse jet produces a thrust of 1.9 kg, however a bigger version of this engine, the giant Chinese valveless engine, produces around 5.4 kg.

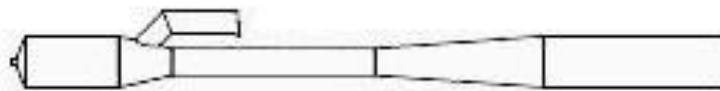


Figure 11 - Chinese CS pulsejet [3].

As the name says, U-shaped engine has the shape of a U (see Fig. 12). It is the configuration of the Lockwood Hiller engine. The advantage of this configuration is shared with the linear since it also has the intake and exhaust pipe pointing in the same direction. The disadvantage is also the loss of the ram-air effect and, because of its shape, it takes up more space. The Lockwood Hiller is one of the largest developed engines and is capable of producing a thrust of 25 kg.

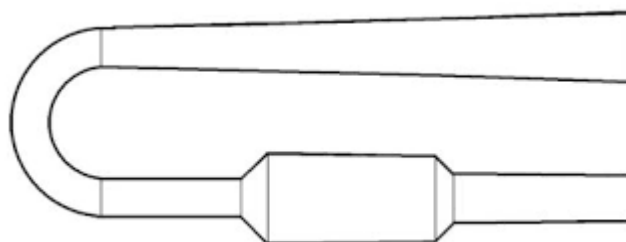


Figure 12 - U-shaped pulsejet [18].

Chapter 3

Numerical Modelling

Over the years, computational power has been improved and now it is possible to work towards a CFD-based analytical design approach. Computational fluid dynamics provides a qualitative prediction of the fluid flows by the mean of mathematical modelling, numerical methods and software tool. CFD simulations were carried using Ansys Fluent 16.2 and mesh was made in Ansys Meshing.

3.1 Governing equations

The motion of a fluid is completely described by the conservation laws for three basic properties: mass, momentum and energy. These three conditions determine the behaviour of the system without any additional dynamical law [26]. The only additional information needed is the specification of the nature of the fluid. Due to high level of generality and degree of abstraction involved, it can be said that this has been one of the greatest achievements of modern science.

The equation for mass conservation is also called the continuity equation, while the momentum conservation law is the expression of the generalized Newton Law, defining the equation of motion of a fluid. The energy conservation law is also referred to as the expression of the first principle of Thermodynamics.

- Continuity equation [27]

The law of mass conservation is independent of the nature of the fluid or of the forces action on it. This law implies that in a fluid system, mass can neither be created or destroyed. No diffusive flux exists for the mass transport, which means that mass can only be transported through convection. With the convective flux defined and in absence of external mass sources, the general continuity equation is:

$$\frac{\partial \rho}{\partial t} + \nabla \cdot (\rho \vec{v}) = 0 \quad (3.1)$$

- Momentum conservation equation [27]

Momentum is a vector quantity defined as the product of density and velocity when expressed per unit of volume. The conservation law will have the general form:

$$\frac{\partial}{\partial t}(\rho \vec{v}) + \nabla \cdot \rho \vec{v} \vec{v} = -\nabla p + \nabla \bar{\tau} + \rho \vec{g} + \vec{F} \quad (3.2)$$

Where p is the static pressure, $\bar{\tau}$ is the stress tensor, $\rho \vec{g}$ is the gravitational body force and \vec{F} correspond to the external forces. The stress tensor is given by:

$$\bar{\tau} = \mu_t \left[(\nabla \vec{v} + \nabla \vec{v}^T) - \frac{2}{3} \nabla \cdot \vec{v} I \right] \quad (3.3)$$

Here, μ is the molecular viscosity, I is the unit tensor and the second term on the right side is the effect of the volume dilation.

- Energy equation [27]

In a fluid, the conserved quantity is the total energy that is defined as the sum of the internal energy and kinetic energy per unit mass. ANSYS Fluent solves the energy equation in the following form:

$$\frac{\partial}{\partial t}(\rho E) + \nabla \cdot (\vec{v}(\rho E + p)) = \nabla \cdot \left(k_{eff} \nabla T - \sum_j h_j \vec{j}_j + (\bar{\tau}_{eff} \cdot \vec{v}) \right) + S_h \quad (3.4)$$

The first three terms on the right side of the equation represent the energy transfer due to conduction, species diffusion and viscous dissipation, respectively. In the first term k_{eff} is the effective conductivity, and in the second term \vec{j}_j is diffusion flux of species j . The S_h term refers to the contributions of the radiation.

3.2 Models

ANSYS Fluent is a very versatile code, and so there are a variety of models that can be chosen, depending on the necessity of the simulation.

3.2.1 Turbulence model

A turbulence model is a semi-empirical equation relating the fluctuating correlation to mean flow variables with various constants provided from experimental investigations.

The turbulence model selected was realizable $k - \varepsilon$ model, which is an improvement and modification of the standard $k - \varepsilon$ model. This new model differs from the standard because it comprehends an alternative formulation for the turbulent viscosity and a modified equation for dissipation rate, ε , based on the dynamic equation of the mean-square vorticity fluctuation. Performance is substantially improved for jets and mixing layers, channels, boundary layers and separated flows compared to the standard $k - \varepsilon$ model [28]. For this model all constants were maintained at the default values.

The modelled equations for k and ε are [27]:

$$\frac{\partial}{\partial t}(\rho k) + \frac{\partial}{\partial x_j}(\rho k u_j) = \frac{\partial}{\partial x_j} \left[\left(\mu + \frac{\mu_t}{\sigma_k} \right) \frac{\partial k}{\partial x_j} \right] + G_k + G_b + \rho \varepsilon + Y_M + S_k \quad (3.5)$$

$$\frac{\partial}{\partial t}(\rho \varepsilon) + \frac{\partial}{\partial x_j}(\rho \varepsilon u_j) = \frac{\partial}{\partial x_j} \left[\left(\mu + \frac{\mu_t}{\sigma_\varepsilon} \right) \frac{\partial \varepsilon}{\partial x_j} \right] + \rho C_1 S_\varepsilon - \rho C_2 \frac{\varepsilon^2}{k + \sqrt{\nu \varepsilon}} + C_1 \frac{\varepsilon}{k} C_3 G_b + S_\varepsilon \quad (3.6)$$

Where, G_k is the turbulence kinetic energy due to the mean velocity gradients, G_b is the turbulence kinetic energy due to buoyancy and Y_M is the contribution of the fluctuating dilatation in compressible turbulence to the overall dissipation rate. The terms C_2 , $C_{1\varepsilon}$ are constants, S_k and S_ε are user-defined source terms and σ_k and σ_ε are the turbulent Prandtl number for k and ε , respectively. C_1 is given by:

$$C_1 = \max \left[0,43; \frac{\eta}{\eta + 5} \right] \quad (3.7)$$

Where,

$$\eta = S \frac{k}{\varepsilon}, \quad S = \sqrt{2S_{ij}S_{ij}} \quad (3.8)$$

The turbulent viscosity is calculated by the following equation:

$$\mu_t = \rho C_\mu \frac{k^2}{\varepsilon} \quad (3.9)$$

3.2.2 Species model

For the species, it was chosen the non-premixed combustion model. In this model fuel and oxidizer enter the reaction zone in distinct streams (see fig. 13). In this model, it is necessary to generate a PDF (Probability Density Function) table which contains information on the thermochemistry and its interaction with turbulence. Under certain assumptions, the thermochemistry can be reduced to a single parameter: the mixture fraction. The mixture fraction, denoted by f , is the mass fraction that originated from the fuel stream, $f=1$ in fuel stream and $f=0$ in oxidizer stream.

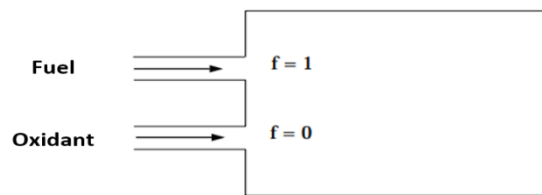
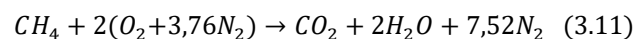


Figure 13 - Non-premixed combustion [27].

It was said before that pulsejet engine can run in a wide range of fuels. For the present study were selected propane (C_3H_8) and methane (CH_4), which are the two more widely used fuels reported in bibliography. For a stoichiometric mixture and complete combustion, the combustion reaction can be described by:



In modelling the non-premixed combustion inlet diffusion was selected, enabling the diffusion flux of species at the flow inlet. The compressibility effects were also selected: this option tells

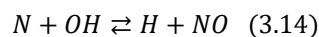
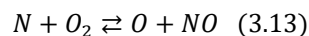
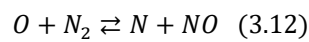
Fluent to update the density, temperature, species mass fraction, and enthalpy from the PDF tables to account for the varying pressure of the system. In the chemistry tab, chemical equilibrium is selected and as for the energy treatment, non-adiabatic is enabled.

The Fuel Stream Rich Flammability Limit allows a “partial equilibrium” calculation, suspending equilibrium calculations when the mixture fraction exceeds the specified rich limit. This increases the efficiency of the PDF calculation, avoiding the complex equilibrium calculations in the fuel-rich region. This is also more physically realistic than the assumption of full equilibrium. For combustion cases, it is normal to choose a value between 10% to 50% larger than the stoichiometric mixture fraction [27]. In this study it was chosen a value 20% larger, the stoichiometric fraction for propane and methane are 0,0641 and 0,0583 respectively, thus the fuel stream rich flammability limit was set to 0,07692 and 0,06993.

3.2.3 NO_x formation

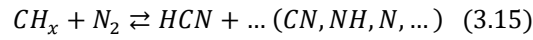
When non-premixed combustion model is selected, it is possible to enable the NO_x model, otherwise ANSYS Fluent will not display any information related with the formation of NO_x . The formation of NO_x can be attributed to four distinct chemical kinetic processes: thermal NO_x formation, prompt NO_x formation, fuel NO_x formation, and intermediate N_2O [27]. Thermal NO_x is formed by the oxidation of atmospheric nitrogen present in the combustion air and prompt NO_x is produced by high-speed reactions at the flame front. The other two mechanisms were not considered in this study as they would not affect the NO_x formation.

The formation of thermal NO_x is associated to a high temperature-dependent chemical reaction. Thermal NO_x is predominant in combustion system where the flame temperature is greater than 1800 K. Its formation will increase with increasing oxygen concentration and it is highly dependent of the temperature, but independent of the fuel type [29]. The three principal reactions governing the formation of thermal NO_x are known as the extended Zeldovich mechanism. The reaction described in 3.12 corresponds to the formation of thermal NO_x , particularly at near-stoichiometric conditions and in fuel-rich mixtures.



Prompt NO_x can be formed in a significant quantity in some combustion environments, such as in low-temperature, fuel-rich conditions and where residence times are short. It is associated

to the reaction of molecular nitrogen (N_2) with hydrocarbon radicals present in flame (C , CH , CH_2 , ...). The general reaction is given by:



The products of these reactions could lead to formation of amines and cyano compounds that subsequently react to form NO .

3.2.4 Radiation

Radiation is one important heat transfer phenomenon in combustion devices because of the high temperature achieved in the system. Previous studies have shown that it is necessary to solve radiative heat transfer to improve combustion simulation results, otherwise the results might have a significant error associated [30].

The P-1 radiation model is the simplest case of the more general P-N model, which is based on the expansion of the radiation intensity into an orthogonal series of spherical harmonics [27].

As P-1 model is the simplest case, the radiation flux can be described by only four terms:

$$q_r = -\frac{1}{3(a + \sigma_s) - C\sigma_s} \nabla G \quad (3.16)$$

Where a is the absorption coefficient, σ_s is the scattering coefficient, G is the incident radiation and C is the linear-anisotropic phase function coefficient. This equation can be simplified by introducing the parameter:

$$\Gamma = \frac{1}{3(a + \sigma_s) - C\sigma_s} \quad (3.17)$$

The equation for radiation flux is:

$$q_r = -\Gamma \nabla G \quad (3.18)$$

The transport equation G is:

$$\nabla \cdot (\Gamma \nabla G) - aG + 4an^2\sigma T^4 = S_G \quad (3.19)$$

Where n is the refractive index of the medium, σ is the Stefan-Boltzmann constant and S_G is a user-defined radiation source. ANSYS Fluent solves this equation to determine the local radiation intensity when P1 model is activated.

Combining equations 3.21 and 3.22 it gives the following equation:

$$-\nabla \cdot q_r = aG - 4an^2\sigma T^4 \quad (3.20)$$

The expression for $-\nabla \cdot q_r$ can be directly substituted into the energy equation to account for heat sources due to radiation.

3.3 Near wall treatment

Turbulent flows are significantly affected by the presence of walls. Obviously, the mean velocity field is affected through the no-slip condition that must be satisfied at the wall. However, the turbulence is also changed by the presence of the wall in non-trivial ways. Very close to the wall, viscous damping reduces the tangential velocity fluctuations, while kinematic blocking reduces the normal fluctuations. Towards the outer part of the near-wall region, however, the turbulence is rapidly increased by the production of turbulence kinetic energy due to the large gradients in mean velocity.

The near-wall modelling significantly impacts the fidelity of numerical solutions, since walls are the main source of mean vorticity and turbulence. After all, it is in the near-wall region that the solution variables have large gradients, and the momentum and other scalar transports occur most vigorously. Therefore, accurate representation of the flow in the near-wall region determines successful predictions of wall-bounded turbulent flows.

There are two approaches to modelling the near-wall region: wall functions and near wall modelling (see Fig. 14) [31]. In the first approach, the viscosity-affected inner region is not resolved, the wall functions are used to bridge the viscosity-affected region between the wall and the fully-turbulent region. In another approach, the turbulence models are modified to enable the viscosity-affected region to be resolved with a mesh all the way to the wall.

In most high-Reynolds-number flows, the wall function approach substantially saves computational resources, because the viscosity-affected near-wall region, in which the solution

variables change most rapidly, does not need to be resolved. The wall-function approach is popular because it is economical, robust, and can be reasonably accurate. However, is inadequate in situations where the low-Reynolds-number effects are pervasive and the assumptions underlying the wall functions cease to be valid. Such situations require near-wall models that are valid in the viscosity-affected region and accordingly integrable all the way to the wall.

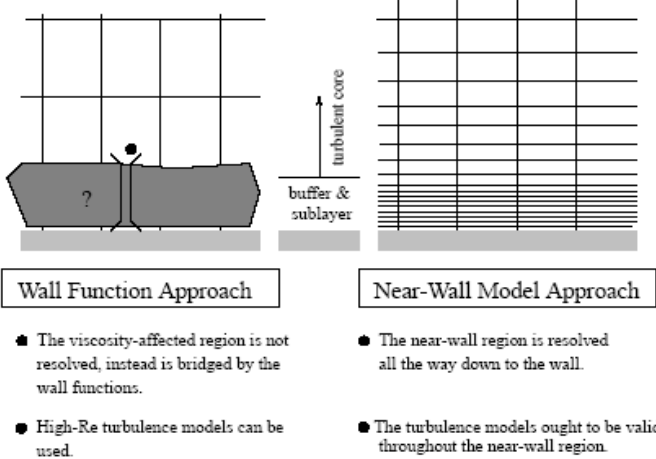


Figure 14 - Near wall treatment [31].

Chapter 4

Methodology

4.1 Sizing procedure

Valveless pulsejet is one of the simplest jet engines, nonetheless it is still challenging to fully understand its operation. In literature is difficult to find relations or equations that permit to do an initial sizing for valveless pulsejet. However, for valved pulsejet there is a set of equations that allows an initial sizing of the engine parts. In this project, a calculation procedure is developed to determine the main dimensions for this type of engine. At the same time, there were already some defined relations based on existing pulsejets.

According to some references, the first step in valveless pulsejet sizing was to establish a relation between the thrust and the volume of the combustion chamber [32] [33]. In Table 1 these parameters of existing engines are shown.

Table 1 - Pulsejet thrust and combustion chamber volume.

Name	F [kg]	V _{cc} (m ³)
Giant Chinese Valveless	5.443108	0.001514
Advanced focused wave	1.020583	0.000344
Lockwood Hiller	24.94758	0.008823
Chinese	1.9	0.000283
Lady Anne	1.3	0.000369
Thermojet Style	1.133981	0.000273
FWE Twin Stack	1.814369	0.000334

Through these parameters the following relationship was reached:

$$F = 2735.1V_{cc} + 0.892 \quad (4.1)$$

The next step was to determine the diameters, once again based on the existing engines. Table 2 shows the diameters of the pulsejets and the areas of the intake and the exhaust pipe. It is important to refer that these areas are the closest to the combustion chamber. With these

data, it was possible to find the ratio between the exhaust and intake pipes areas, and the combustion chamber volume with the exhaust areas. The average of the obtained ratios was calculated. Using equation 4.1 it is possible to know combustion chamber volume, and with this value and the average of A_{ex}/A_{in} and V_{cc}/A_{ex} can be calculated the exhaust and the intake diameters for a known thrust. The intake tube's internal diameter should be around three fourths of the exhaust's internal diameter [11].

Table 2 - Pulsejet engines parameters.

Name	(A_{ex}/A_{in})	V_{cc}/A_{ex}
Giant Chinese Valveless	1.346745	0.845382
Advanced focused wave	2.323766	0.434488
Lockwood Hiller	0.64	1.944909
Chinese	1.137778	0.558508
Lady Anne	1.935728	0.458814
Electra II	2.777778	-
IAME Escopeta	1	0.494225
Thermojet Style	3.125	0.344814
FWE Twin Stack	1.000595	1.214859
MATS University	0.000789	3.115165
Average	1.840255	0.685984

Then it was necessary establish relations to find the lengths. For valaveless pulsejet no reference was found mentioning any method whatsoever. Even so, for valved pulsejet Tharratt settled equations that relate the mean engine area with thrust and the engine total length with the mean diameter [20]. Valved engine was treated as a straight duct so this relation could be applied. Given the fact that for valeveless pulsejet lengths was not found any refence, it will be tested the veracity of this relations for valveless engines.

$$F = 1546.753A_m \quad (4.2)$$

Tharratt also stated that, for ratios between the total length and the mean diameter lower than 7, the development problems are particularly challenging. With this two information the mean diameter was calculated taking into account the mean area which is determined using equation 4.2.

Based on Table 3 and Table 4 was obtained a relation between the total length and the mean diameter. The total length of the engines was considered as the sum of the combustion chamber and the exhaust pipe lengths, only in the case of IAME Escopeta the intake length contributes

for the overall length. This ratio meets the Tharratt requirement of being higher than 7 and allows us to obtain the total length of the engine.

Table 3 - Pulsejet mean areas and diameters.

Name	F [kg]	A _m [m ²]	D _m [m]
Giant Chinese Valveless	5.443108	0.003519	0.066937
Advanced focused wave	1.020583	0.00066	0.028985
Lockwood Hiller	24.94758	0.016129	0.143304
Chinese	1.9	0.001228	0.039548
Lady Anne	1.3	0.00084	0.032713
Thermojet Style	1.133981	0.000733	0.030553
FWE Twin Stack	1.814369	0.001173	0.038646
MATS University	3.5	0.002263	0.053676

Table 4 - Pulsejet engine lengths.

Name	L _{ex} [m]	L _{in} [m]	L [m]
Giant Chinese Valveless	1.0668	0.21844	1.35255
Advanced focused wave	0.4318	0.128905	0.619125
Chinese	0.665163	0.14605	0.828675
Lady Anne	0.347	0.129	0.549
Electra II	0.508	0.11684	0.5842
IAME Escopeta	1.74	0.446	2.836
Thermojet Style	0.4064	0.0762	0.555625
FWE Twin Stack	0.361	0.14	0.56
MATS University	0.3683	0.0762	0.4699

$$\frac{L}{D_m} = 17.26 \quad (4.3)$$

A crucial element in the design of a pulsejet is the combustion chamber. The design chosen is conical, as shown in figure 15. In the sizing of this component there are three variables which must be determined: major radius, total length and the end cup length. It was found the average of the ratios between the major and the minor diameter of the existing designs, as seen in the Table 5, and it agrees with other studies which state that the exhaust tube's internal diameter should be half of the major combustion chamber's internal diameter [11]. It should be noted that the minor radius of the combustion chamber is equal to the radius of the exhaust pipe for the chosen design.

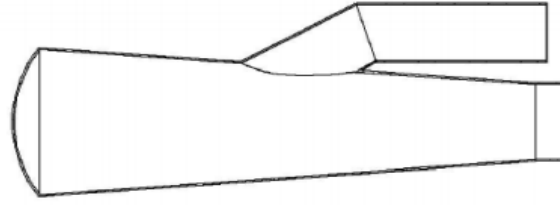


Figure 15 - Pulsejet combustion chamber design [33].

Table 5 - Diameter ratio.

Name	D _{cc} [m]	D _{ex} [m]	Ratio
Giant Chinese Valveless	0.0889	0.047752	1.8617
Advanced focused wave	0.0635	0.03175	2
Chinese	0.0508	0.0254	2
Lady Anne	0.064	0.032	2
IAME Escopeta	0.12	0.07	1.714286
Thermojet Style	0.08255	0.03175	2.6
FWE Twin Stack	0.064	0.029	2.206897
Average			2.054698

A function to relate the end cup volume to the total volume of the combustions chamber was also determined. It was verified that the end cup volume corresponds to about 3,7% of the total volume.

$$V_{cup} = 0.037V_{CC} \quad (4.4)$$

After this dimensioning, the length of the end cup and the total length of the combustion chamber can be now determined using the formula of the spherical cap and cone trunk volumes.

At last, with the dimension of the combustion chamber defined, is possible to find the intake and the exhaust pipe lengths. As stated above, the total length was the sum of the combustion chamber and the exhaust pipe length, and so it can now be obtained the exhaust pipe length. According to the dimensions of the existent engines, the intake length was assumed as linear function of the total length:

$$L_{in} = 0.159914L + 0.019354 \quad (4.5)$$

4.1.1 Initial sizing

According to the formulas defined in the previous sub-chapter it is possible to draw a design based on a selected thrust. The design was chosen based on the advanced focused wave type, which is a linear configuration, due to its simplicity. In the developed calculation routine, all the variables depend on the thrust value, for which it must be the first variable to be defined. In this project it was selected a value that fit the range of the thrust values of the engines used, so the thrust chosen was 6 kg. Based on that, the initial sizing of the engine is presented in Table 6 and an isometric view is also showed in Figure 16. Dimensions are also presented in detail in appendix A.

Table 6 - Pulsejet dimensions.

Intake	Radius	0.02169 m
	Length	0.2133 m
	Angle	148°
Exhaust	Radius	0.02942 m
	Length	0.9173 m
	Flare	0.0326 m
Combustion Chamber	Minor radius	0.02942 m
	Major radius	0.05884 m
	Length	0.2832 m
	End cup length	0.01224 m
	Fuel injector radius	0.003 m

According to the results shown in Table 6, the ratio between the diameters of the intake and exhaust pipe agreed with the statement of Kudesia and Bisen [11].

A flare 10% bigger than the exhaust pipe diameter was also included: studies proved that the presence of a flare at the end of the exhaust pipe improved the pulsejet operation, as it helps to start the pulsing action more quickly and allows a higher pick pressure in the combustion chamber [13]. The intake angle was selected based on the original advanced focused wave pulsejet. The draughting was made using the software CATIA V5.

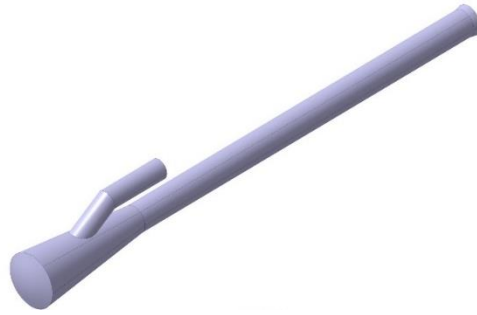


Figure 16 - Pulsejet isometric view.

4.2 Generation of numerical mesh

The partial differential equations that govern fluid flow and heat transfer are not usually agreeable to analytical solutions, except for very simple cases. Therefore, to analyse fluid flows, flow domains are divided into smaller subdomains. The governing equations are then discretized and solved inside each of these subdomains. It must be guaranteed proper continuity of solution across the common interfaces between two subdomains to ensure that the various solutions can be combined and can give a full picture of the entire domain. The subdomains are often called elements or cells, and the group of all elements or cells is called a mesh or grid.

To obtain good results in CFD simulation it is important to have an appropriate mesh. The precision of the results obtained depends on the refinement of the mesh, finer mesh leads to more accurate results, albeit taking more time. There is a point where having a finer mesh is not beneficial because the results start to be similar independently of the mesh refinement. To find this point, it is important to do a study of the mesh, which is called mesh independence. This method consists in improving the number of the mesh elements according to a defined factor until the solution reaches an aim. This aim can be an error in relation to a reference or can be an error related with the previous results, which shows that even with a more refined mesh the solutions does not change significantly.

In mesh independence study, for the three different meshes obtained, it was evaluated the pressure inside the combustion chamber. A selected point in the combustion chamber allowed an analysis of the pressure for both the mesh study and engine performance. The results of the mesh independence are detailed in Table 7. The difference between mesh 2 and 3 is much lower than the difference between mesh 1 and 2, because the values are converging to a value and the variances are no longer significant, so mesh 2 was selected. A closer view of the mesh is presented in appendix B.

Table 7 - Mesh independence study.

	Mesh 1	Mesh 2	Mesh 3
Nodes	9567	14820	28822
P _{cc}	91756	92118	92236

4.3 Problem setup

In this study was preferred a 2D transient simulation. A time-dependent simulation was selected in order to observe all the stages of the pulsejet operation: filling, combustion, exhaust and refilling. Furthermore, it turned out helpful to evaluate overall performance of the pulsejet. Initially a 3D study of the pulsejet was performed. However, at an early stage it became difficult to reach the pulsating effect and this type of simulation was computationally expensive. Thus, in order to perform more tests and achieve the pulsating effect, a 2D simulation was preferred.

When initiating ANSYS Fluent it is necessary to ensure that 2D simulation is selected, and it is also necessary so choose between single or double precision. Double precision gives more accurate results, but it will take more time to run. For a 2D simulation, the computational time is no longer a major problem, so double precision was enabled. The simulation can be performed with single or parallel solver, in which the second alternative reduces the computational time since it becomes possible to choose more than one CPU. The computer used had 8 CPUs, so, parallel option was chosen.

Once ANSYS Fluent is launched, it is important to check the mesh quality, as it affects the results. It must also be checked if there are negative cell volumes, since it tells whether there are degenerated cells in the mesh - this was not the case. When reporting mesh quality there are three important parameters: aspect ratio, orthogonal quality and skewness. The values for them are 14.5, 0.6718 and 0.3282, respectively. According to the mesh metrics spectrum given by ANSYS Fluent these values represent a good mesh [34].

4.3.1 Boundary conditions

Boundary conditions are necessary constraints that specify the flow and thermal variables on the boundaries of a physical model, their correct implementation is crucial to obtain good results.

Initially it was established that a stoichiometric fuel-air mixture was admitted directly into the engine through the intake tube, so no fuel stream was defined. However, under these conditions the pulsating effect did not occur. After the combustion started, when the hot gases begin to

be expelled, the intake tube reached very high temperatures, for which the new mixture was immediately burned, never reaching the combustion chamber. After several simulations and varying some factors, was concluded that the fuel should be directly injected into the combustion chamber. The injector was then placed in the middle of the end cup.

It has been established that the air inlet is a pressure inlet, with the total pressure set to zero. The mean mixture fraction is zero, since there is only oxidizer admitted through it, and the temperature is 300 K.

Fuel inlet was set as a mass flow inlet. The fuel is injected at atmospheric pressure, mean mixture fraction is one since it is a fuel stream. One of the aims with this study was observing the variations of different variables according to the change of the fuel mass flow, so different mass flows were tested for both fuels: 0.04 kg/s, 0.06 kg/s, 0.1 kg/s and 0.12 kg/s. These values were chosen after several tests were run, in order to observe which values would work for both fuels. One of the difficulties in the elaboration of this work was precisely this: to find the range of values for which the engine would work. In the literature the range of values used for the fuel mass flow is very large, it varies between 3 mg/s and 30 kg/s [10] [35].

Outlet is defined as a pressure outlet. The static pressure is zero and the backflow temperature 300 K.

The walls were assumed as convective with a heat transfer coefficient of 20 W/m²K. In previous study it was observed that when modelled as an adiabatic boundary the pulsating effect was not observed [29]. This agrees with experimental researches that proved that when the temperature is too high, the engine may fail, or it may lead to a premature ignition which causes the pulse cycle to disappear [36].

It is important to notice that for all flows, ANSYS Fluent uses gauge pressure internally. Any time an absolute pressure is needed, it is generated by adding the operating pressure to the relative pressure.

$$P_{abs} = P_{op} + P_{Gauge} \quad (4.6)$$

4.4 Solution

4.4.1 Solution methods

Ansys Fluent allows to choose one of the two numerical methods:

- pressure-based solver
- density-based solver

In both methods the velocity field is obtained from the momentum equations. In the density-based approach, the continuity equation is used to obtain the density field while the pressure field is determined from the equation of state.

On the other hand, in the pressure-based approach, the pressure field is extracted by solving a pressure or pressure correction equation, this one obtained by manipulating continuity and momentum equations.

Historically speaking, the pressure-based approach was developed for low-speed incompressible flows, while the density-based approach was mainly used for high-speed compressible flows. However, both methods have recently been extended and reformulated to solve and operate for a wide range of flow conditions beyond their traditional or original intent. For this work, pressure-based solver was selected. This method offered two algorithms: segregated and coupled algorithm.

The pressure-based coupled algorithm solves a coupled system of equations comprising the momentum equations and the pressure-based continuity equation. The remaining equations are solved in a decoupled fashion as in the segregated algorithm.

The pressure-based segregated algorithm uses a solution algorithm where the governing equations are solved sequentially (i.e., segregated from one another). Because the governing equations are non-linear and coupled, the solution loop must be carried out iteratively in order to obtain a converged numerical solution.

In coupled algorithm the rate of solution convergence significantly improves when compared to the segregated algorithm. However, the memory requirement increases by 1.5 - 2 times that of the segregated algorithm since the discrete system of all momentum and pressure-based continuity equations needs to be stored in the memory when solving for the velocity and pressure fields. For this reason, the segregated algorithm was used.

With the segregated algorithm, each iteration consists of the following steps [27]:

1. Update fluid properties based on the current solution;
2. Solve the momentum equations, one after another, using the recently updated values of pressure and face mass fluxes;
3. Solve the pressure correction equation using the recently obtained velocity field and the mass-flux;
4. Correct face mass fluxes, pressure, and the velocity field using the pressure correction obtained from step 3;
5. Solve the equations for additional scalars, if any, such as turbulent quantities, energy, species, and radiation intensity using the current values of the solution variables;
6. Update the source terms arising from the interactions among different phases;
7. Check for the convergence of the equations.

When using the pressure-based solver, ANSYS Fluent uses a pressure-velocity coupling algorithm which combines the continuity and momentum equations to derive an equation for pressure (or pressure correction). Pressure-Implicit with Splitting of Operators (PISO) is useful for unsteady flow problems: it takes a little more CPU time per solver iteration, but it can dramatically decrease the number of iterations required for convergence.

Gradients are needed not only for constructing values of a scalar at the cell faces, but also for computing secondary diffusion terms and velocity derivatives. The gradient of a given variable is used to discretize the convection and diffusion terms in the flow conservation equations. Least-Squares Cell-Based minimizes false diffusion and gives more accurate flow solution.

In terms of discretization, second-order upwind was selected due to its accuracy. By default, ANSYS Fluent stores discrete values of the scalar at the cell centres. However, face values must be interpolated from the cell centre values. This is accomplished using an upwind scheme. Upwinding means that the face value is derived from quantities in the cell upstream, or “upwind,” relative to the direction of the normal velocity.

4.4.2 Solution controls

The pressure-based solver uses under-relaxation of equations to control the update of computed variables at each iteration. This means that all equations solved using the pressure-based solver will have under-relaxation factors associated with them. Normally, for combustion simulations, the default values are too aggressive, and this case was no exception. After several tests, the under-relaxation factors were defined as shown in Table 8.

Table 8 - Under-relaxation factors.

Pressure	0.3
Density	0.8
Body forces	1
Momentum	0.7
Turbulent kinetic energy	0.7
Turbulent dissipation rate	0.7
Turbulence viscosity	0.9
Energy	0.9
Pollutant no	0.9
Temperature	1
P1	0.8
Mean mixture fraction	1
Mean mixture fraction variance	0.9

4.4.3 Monitors

Convergence of the solution is a very important aspect in a CFD simulation. A converged solution might not mean a correct one, but it does mean that the results agree with all the parameters assigned in the problem setup. The convergence criteria were maintained at the default value. It is important to observe the residuals behaviour, however in transient solution they do not give enough information to evaluate whether the solution is converging or not. So, it is essential to create monitors for variables of interest and observe if they converge at each time-step.

4.4.4 Solution initialization and calculation set-up

ANSYS Fluent provides two different initialization methods: Standard and hybrid initialization. In this study the second method was chosen.

Hybrid Initialization is a collection of recipes and boundary interpolation methods. It solves the Laplace equation to produce a velocity field that conforms to complex domain geometries, and a pressure field which smoothly connects high- and low-pressure values in the computational domain. All other variables (that is temperature, turbulence, VOF, species, and so on) will be patched based on domain averaged values or a predetermined recipe.

The simulation was started with a low pressure inside the combustion chamber (see Fig. 17), in order to force the air to enter in the combustion chamber. To save computational time, the simulation was initiated with the engine full of fuel (i. e. with the mean mixture fraction set to one).

There are three different ways to ignite the mixture in an initial phase: a spark ignition (though this option is not available in non-premixed combustion model); patch a specified zone with high temperature; or initialize the simulation with a high temperature in the entire domain. In this study, the simulation was initialized with a temperature of 1000 K.

For calculation set-up it is important to first check the case and see if there is any error with the case. Then, the time stepping method selected was fixed with a time step size of 0.0001 s. The number of time steps is 2000 and it was defined a maximum iteration per time step of 20 to ensure a convergence at each time step. The pulsating effect for all the cases started at an early stage, however the simulation only started to stabilize around the 1500-time steps. This means the difference between the value of the variables only started to have an insignificant value from this time step. Therefore, it was selected a time step above that, so the reported values were in an already stable phase of the simulation.

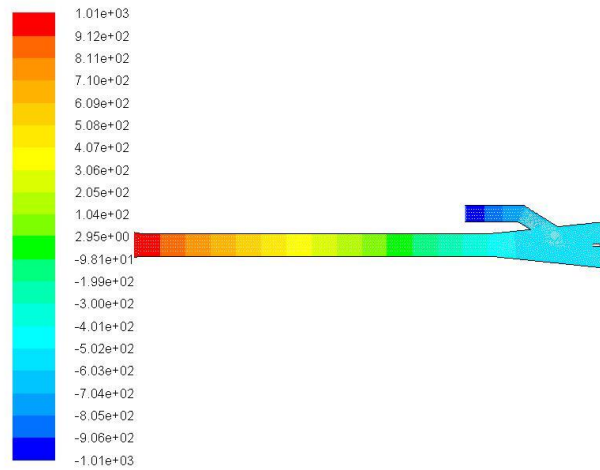


Figure 17 - Initial pressure distribution.

4.5 Thrust calculation

Thrust is a mechanical force which is generated through the reaction of accelerating a mass of gas, as explained by Newton's third law of motion. In fluid dynamics the change in momentum across the propulsion device can be expressed as the change in the mass flow rate times the velocity:

$$F = \dot{m}_{ex}V_{ex} \quad (4.7)$$

There is an additional effect that must be taken into account: the exit pressure being different from the free stream pressure. If there is a net change of pressure in the flow, there is an additional change in momentum. Normally, the magnitude of the pressure-area term is small relative to the $\dot{m}_{ex}V_{ex}$ term. The general thrust equation is then given by:

$$F = \dot{m}_{ex}V_{ex} + (p_{ex} - p_0)A_{ex} \quad (4.8)$$

In this study the equation 4.8 was used to calculate the thrust produced by the engine. As said before, an advantage of valveless pulsejet is the fact that having the intake in same direction as the exhaust pipe makes the thrust generated by the intake pipe contributing to the total thrust. Thus, the total thrust produced by the engine is the sum of the calculated thrust at the inlet and outlet.

When calculating the thrust there is another aspect that must be taken into account. The mass flow rate is given by:

$$\dot{m} = \rho VA \quad (4.9)$$

Since this is a 2D simulation, ANSYS Fluent assumes a virtual area given by the length of the inlet and the outlet, so the mass flow rate will be different for a 3D case. So, in order to calculate the thrust, it is mandatory to calculate the mass flow rate for the 3D case, otherwise the results will be very high since the area assumed by ANSYS Fluent is much larger than the real area. The equation that relates the 2D and 3D mass flow rate is:

$$\dot{m}_{2D} = \dot{m}_{3D} \frac{H \cdot L_{ref}}{A_{3D}} \quad (4.10)$$

Where, H is the height of the port, L_{ref} is ANSYS Fluent reference for 2D planar cases (which is 1 m by default) and A_{3D} is the area of the port in 3D.

Chapter 5

Results

In this chapter, will be presented the results obtained in CFD simulation, starting by the results for the different fuel mass flow of each fuel, and afterwards by a comparison of the performance for both fuels. Initially, six different cases were studied, however it was necessary to do an additional case for propane. For clarity purposes, each one was assigned a letter from A to G. Since A, B, C and D correspond respectively to 0.04, 0.06, 0.1 and 0.12 kg/s for propane and E, F and G are 0.04, 0.06, and 0.1 kg/s for methane.

The first part of this work focused on the sizing of the valveless pulsejet engine. As there were no sizing procedures reported in the literature, was elaborated one based on data of existing engines. Therefore, was necessary to evaluate whether the initial sizing of the engine was working, otherwise it would be necessary to redo it. To validate the operation, is mandatory to observe two phenomena: the pulsating effect and a self-sustaining combustion. In all simulation these two phenomena were observed, and the results of the pulsejet performance will be presented in the next section.

The convergence of the results at each time-step was guaranteed.

5.1 y^+ analysis

The value of y^+ is a dimensionless wall distance, which in CFD is used in turbulence models that need the wall distance for modelling.

It is important in turbulence modelling to determine the proper size of the cells near domain walls. The turbulence model wall laws have restrictions on the y^+ value at the wall. For instance, the realizable $k - \varepsilon$ model requires a wall y^+ value between 30 to 300.

The y^+ value is dependent on the local fluid velocity, which varies across the wall significantly. As this study is a transient simulation, the velocity of the fluid also varies over time. For all simulations, the mean value of y^+ was measured to ensure that it was within the required range. In Figure 18 is represented the mean y^+ for all cases.

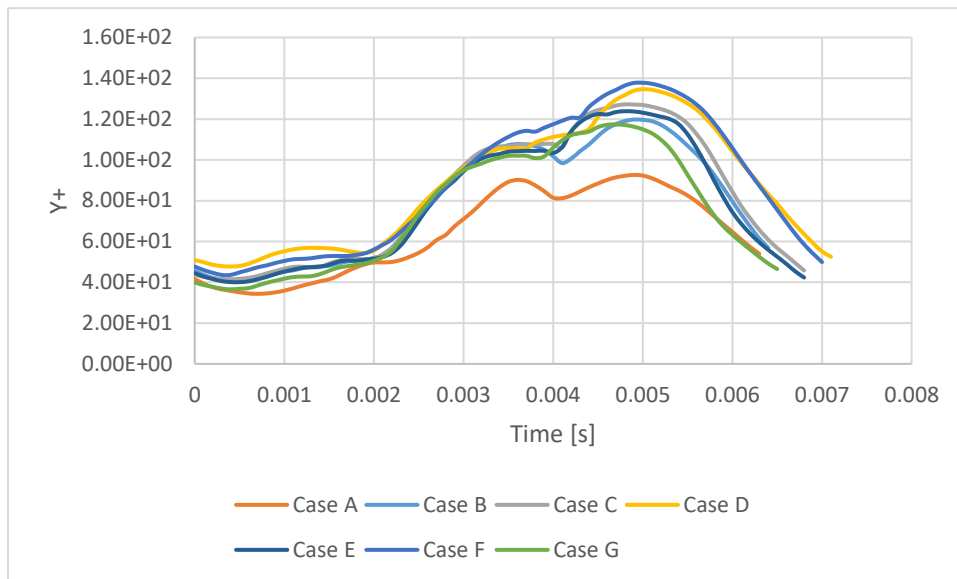


Figure 18 - y^+ variation during a cycle.

5.2 Propane

In literature, propane is the most reported fuel for the use in pulsejet engine, valved or valveless. A major advantage of using propane fuel is that it is relatively cost effective.

Can be seen from the figures 19 and 20, that was possible to achieve the pulsating effect and can be seen all phases of the pulsejet cycle: intake, combustion and exhaustion.

For these two cases different results were obtained, as was expected. In terms of the temperature, it should be noted that, there is a mass of cold air that will only be expelled in the next cycle. This causes the average temperature of this cycle to greatly decrease, which will affect the engine performance. This situation repeats cyclically, so, for lower fuel mass flow, its performance is inconsistent. The results presented in Table 9 and Table 10 are for two consecutive cycles. Is difficult to draw conclusions for these cases since there are significant variation of the variables between the two cycles, however, it is verified that these differences are more accentuated for case A. Due to this, an additional case was studied for propane in order to obtain information to make an evaluation of the influence on the fuel mass flow for this fuel.

- Case A

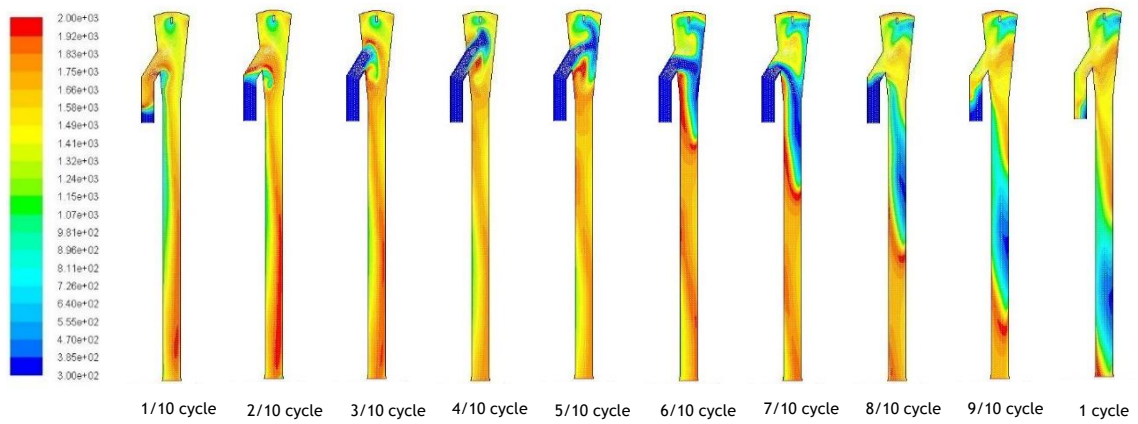


Figure 19 - Temperature contour for case A.

Table 9 - Obtained results for case A.

Peak pressure in combustion chamber [Pa]	8.02e+04	8.50e+04
Minimum pressure in combustion chamber [Pa]	-1.88e+04	-2.08e+04
Maximum exhaust velocity at outlet [m/s]	418	486
Maximum exhaust velocity at inlet [m/s]	188	238
Maximum intake velocity [m/s]	259	274
Maximum thrust [kg]	1.15	1.45

- Case B

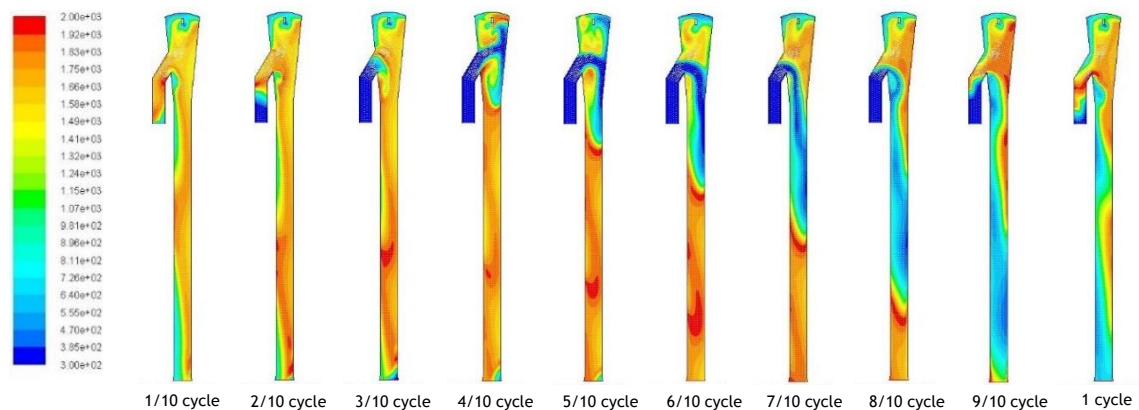


Figure 20 - Temperature contour for case B.

Table 10 - Obtained results for case B.

Peak pressure in combustion chamber [Pa]	8.14e+04	8.30e+04
Minimum pressure in combustion chamber [Pa]	-2.22e+04	-2.50e+03
Maximum exhaust velocity at outlet [m/s]	432	461
Maximum exhaust velocity at inlet [m/s]	157	187
Maximum intake velocity [m/s]	256	252
Maximum thrust [kg]	1.30	1.45

For case C and case D did not occur the same problem as before. In these two cases the variation between cycles are irrelevant, therefore conclusions can be drawn. Exhaustion velocities and the peak pressure in the combustion chamber increase with increasing mass flow rate.

The produced thrust depends mainly on the exhaust velocity and mass flow rate. To what concerns the mass flow rate, it does not show significant variations for the two cases, so the velocity is the principal factor that influences thrust. Since velocity increases with increasing fuel mass flow, case D shows the highest velocity and therefore the highest thrust.

The peak and the minimum pressure in combustion chamber is a very important aspect in the pulsejet operation. Its self-sustaining pulsating combustion is only possible by the pressure differentials. The peak pressure is higher in case D, and this agrees with other studies which also reported that the peak pressure increases with increasing fuel mass flow [10] [35] [37].

In terms of temperature, there does not appear to be a relation between the combustion chamber peak temperature and the fuel mass flow. Nonetheless, the average exhaust temperature both at outlet and inlet is higher for higher fuel mass flow.

Pulsejet engines work in the deflagration of the fuel-air mixture, which is a subsonic combustion. Then, for this work it was also relevant to obtain data on the Mach number in order to verify if the deflagration of the mixture occurred. In tables 11 and 12 the maximum value of Mach number is presented, and although it is quite high it is less than one which confirms the occurrence of a deflagration.

- Case C

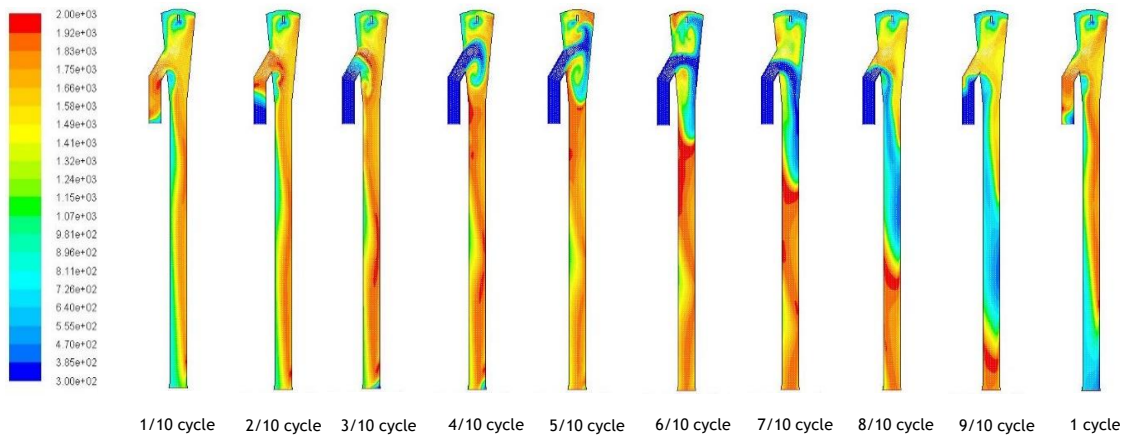


Figure 21 - Temperature contour for case C.

Table 11 - Obtained results for case C.

Peak pressure in combustion chamber [Pa]	9.21e+04
Minimum pressure in combustion chamber [Pa]	-2.09e+04
Maximum exhaust velocity at outlet [m/s]	493
Maximum exhaust velocity at inlet [m/s]	205
Maximum intake velocity [m/s]	267
Maximum thrust [kg]	2.14
Maximum Mach number	0.91

- Case D

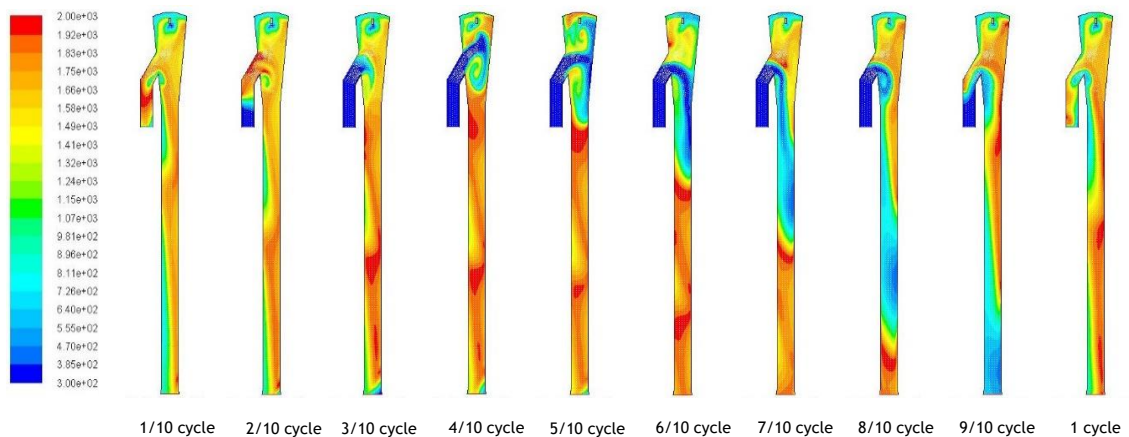


Figure 22 - Temperature contour for case D.

Table 12 - Obtained results for case D.

Peak pressure in combustion chamber [Pa]	9.50e+04
Minimum pressure in combustion chamber [Pa]	-2.07e+04
Maximum exhaust velocity at outlet [m/s]	547
Maximum exhaust velocity at inlet [m/s]	213
Maximum intake velocity [m/s]	263
Maximum thrust [kg]	2.53
Maximum Mach number	0.95

5.3 Methane

For methane as fuel, the pulsating effect was also observed (see Figs. 23 to 25), and the behaviour is very similar to the one reported with propane (see Tables 13 to 15).

When increasing the fuel mass flow, the exhaust velocity at outlet and the intake velocity also increase. On the other hand, the exhaust velocity at inlet does not show a relation with the mass flow.

For the maximum thrust, the conclusions are similar for both fuels. The exhaust velocity is the main factor that influences the produced thrust, so given an increasing fuel flow, the exhaust velocity increases and therefore so does the thrust.

The peak pressure variation is also in agreement with other studies, with increased fuel flow, the peak pressure also increased. The minimum pressure reported is different for the three cases, though its variation does not follow the fuel mass flow variation, being the minimum pressure reported for case F.

The temperature in combustion chamber does not show any relation with the fuel mass flow, as occurred with propane. However, the average temperature at outlet during the cycle increases with increasing fuel mass flow, so the highest average temperature is for case G. The phenomenon observed in propane is not verified with such intensity in this case. Thus, the results for this fuel are more consistent throughout the cycles.

As for propane the data on the maximum Mach number were also analysed. In this case the values are also below one, which confirms the occurrence of the deflagration of the mixture.

- Case E

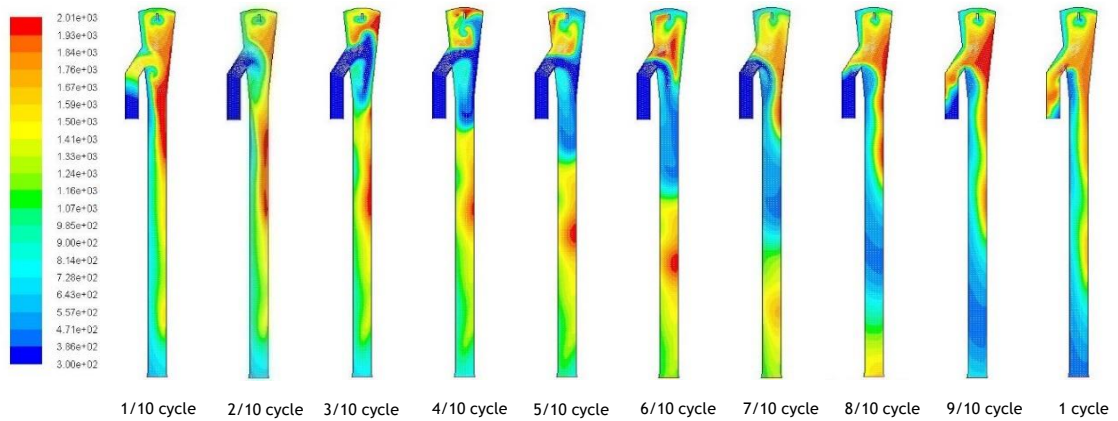


Figure 23 - Temperature contour for case E.

Table 13 - Obtained results for case E.

Peak pressure in combustion chamber [Pa]	7.56e+04
Minimum pressure in combustion chamber [Pa]	-2.00e+04
Maximum exhaust velocity at outlet [m/s]	436
Maximum exhaust velocity at inlet [m/s]	218
Maximum intake velocity [m/s]	251
Maximum thrust [kg]	1.03
Maximum Mach number	0.66

- Case F

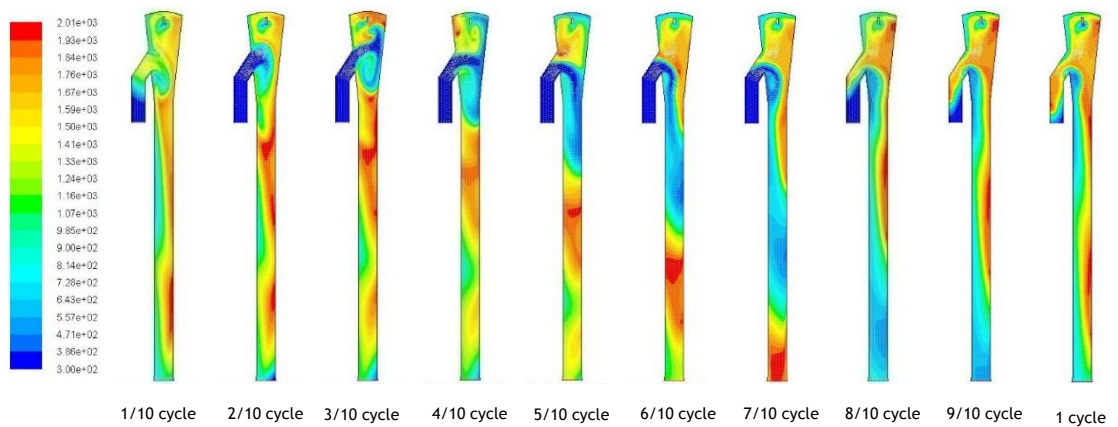


Figure 24 - Temperature contour for case F.

Table 14 - Obtained results for case F.

Peak pressure in combustion chamber [Pa]	8.27e+04
Minimum pressure in combustion chamber [Pa]	-2.20e+04
Maximum exhaust velocity at outlet [m/s]	475
Maximum exhaust velocity at inlet [m/s]	216
Maximum intake velocity [m/s]	264
Maximum thrust [kg]	1.5
Maximum Mach number	0.82

- Case G

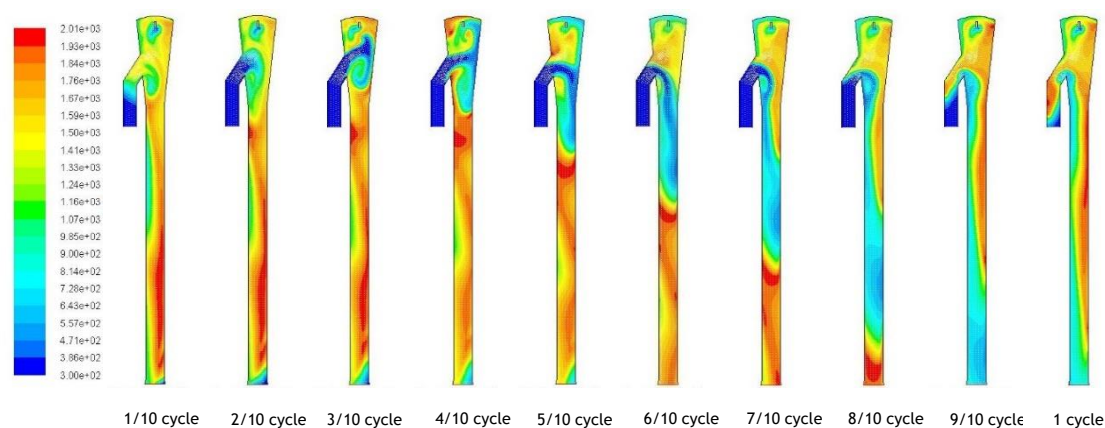


Figure 25 - Temperature contour for case G.

Table 15 - Obtained results for case G.

Peak pressure in combustion chamber [Pa]	9.30e+04
Minimum pressure in combustion chamber [Pa]	-2.12e+04
Maximum exhaust velocity at outlet [m/s]	534
Maximum exhaust velocity at inlet [m/s]	218
Maximum intake velocity [m/s]	269
Maximum thrust [kg]	2.31
Maximum Mach number	0.87

5.4 Emissions analysis

In this subchapter the results on pollutant emissions are presented. In the literature there were no references found related to this subject, so the results obtained will be compared only among them. A comparison will be made for the same fuel for different fuel mass flows and for the two fuels with the same fuel mass flow. The results presented correspond to the emission per cycle and are the sum of the gases exiting the engine by the exhaust and intake pipes.

5.4.1 Carbon monoxide

CO emissions are associated to incomplete combustion. In figure 26 are presented the contours for the *CO* mass fraction in case G. In the exhaust pipe there is a region with a high concentration of *CO*. This may be explained by the fact that the fuel is injected continuously, that is, even when gases are being exhausted the fuel continues to enter the combustion chamber. At this stage there is not enough air in the combustion chamber for a complete combustion, so that excess fuel will be expelled, leading to the high concentration of *CO* in the exhaust pipe.

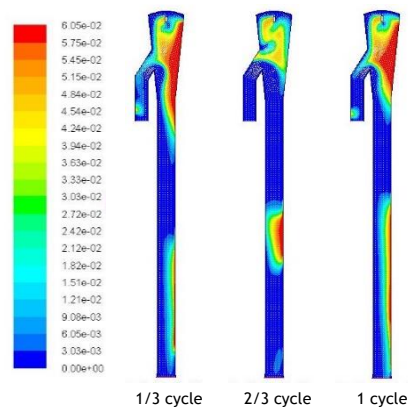


Figure 26 - Contours of CO concentration for case G.

For both fuels the *CO* emission increases when increasing fuel mass flow, as reported in table 16. When comparing methane and propane for the same fuel mass flow (case C and case G) the mass fraction is higher for propane. Methane is a less dense fuel, so it mixes better with air which leads to a more efficient combustion.

Table 16 - Results of CO formation per cycle.

Case	CO Mass fraction
C	2.39e-03
D	6.81e-03
F	1.98e-06
G	1.49e-03

5.4.2 Carbon dioxide

CO_2 are a great part of the exhaust gases, they are the result of complete combustion of fuels, so the only way to reduce them is to burn less fuel. As previously seen, for lower fuel flows the thrust produced is lower. This is one of the today's problem for engineers, produce the same power output for less fuel. When comparing figure 27 with the figure of the temperature contour (see Fig. 25), it is possible to verify that the regions of greater concentration of CO_2 correspond to the regions of higher temperature.

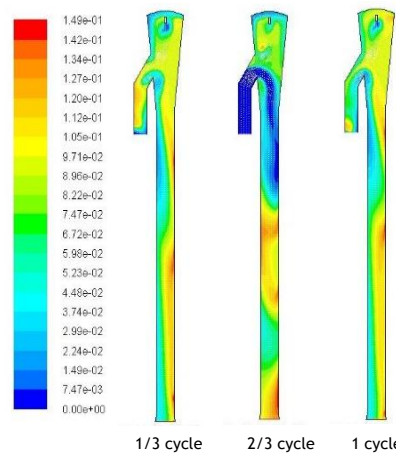


Figure 27 - Contours of CO_2 concentration for case G.

Analysing table 17 is verified that CO_2 emissions increase when increasing fuel mass flow for both fuels. When comparing case C and G the formation of CO_2 is clearly higher for propane.

Table 17 - Results of CO₂ formation per cycle.

Case	CO ₂ Mass fraction
C	4.43e-02
D	5.01e-02
F	2.55e-02
G	3.81e-02

5.4.3 Nitrogen oxides

As explained in section 3.2.3 it was considered the formation of thermal and prompt NO_x, being the thermal NO_x associated with high temperatures and prompt NO_x with fuel richer regions. The results presented in figure 28 account the total NO_x concentration, which is the sum of thermal and prompt NO_x.

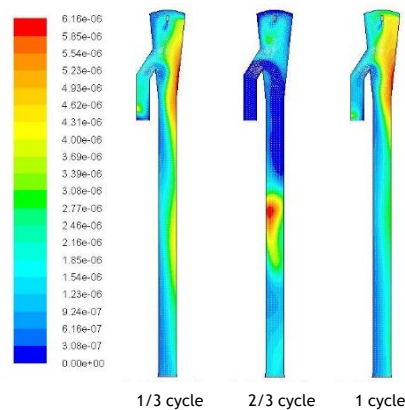


Figure 28 - Contours of NO_x concentration for case G.

In table 18 are presented the results for the four cases. The behaviour of NO_x is equal to that of the pollutants seen before. For higher fuel mass flow, the formation of NO_x is higher, and it is also superior for the propane cases.

Table 18 - Results of NO_x formation per cycle.

Case	NO _x Mass fraction
C	1.18e-06
D	1.27e-06
F	4.14e-07
G	7.47e-07

5.5 Combustion chamber pressure vs thrust

As mentioned before, the pressure changes in the combustion chamber are very important for the operation of the pulsejet. In this sub-chapter is presented a relation between the pressure in the combustion chamber and the thrust produced by the engine during a cycle.

In figures 29 to 33, it is possible to observe negative thrust. This corresponds to the phase of the cycle when the hot gases reverse direction, although this amount of thrust is smaller when compared with the thrust produced by the hot gases leaving the engine.

When comparing these results with the ones reported by Geng et al. [10], is possible to observe the same behaviour of the thrust in relation to the pressure. As the pressure begins to fall below atmospheric, the pulsejet appears to produce a sudden burst of positive thrust. For methane, this phenomenon is more evident for higher fuel mass flow. However, in Geng [10] the thrust oscillation frequency appears to be twice that of the pressure trace and, in this work, both variables show similar frequencies. This difference in results may be explained by the different size of the engines.

As seen in Figures 29 to 33, the maximum thrust obtained was around 2.5 kg, this result being lower than the projected. This engine was designed having on mind a produced thrust of 6 kg. Although the results obtained were lower than the expected, they fit in the range of the thrust produced for engines with similar dimensions [33].

In this sub-chapter cases A and B were not presented since they did not contain relevant information, however, the same behaviour was verified: and increase in thrust was observed when the pressure drops below atmospheric.

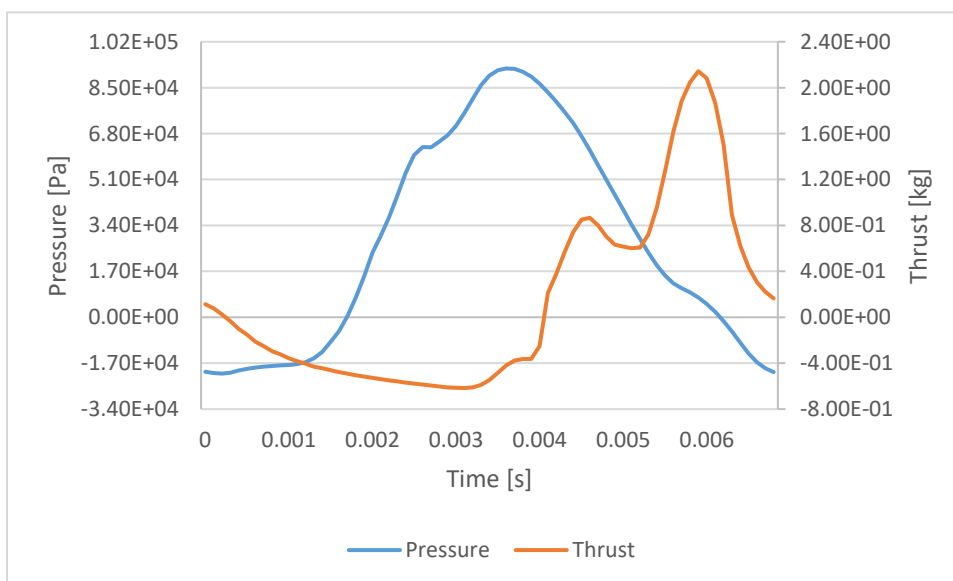


Figure 29 - Combustion chamber pressure vs thrust for case C.

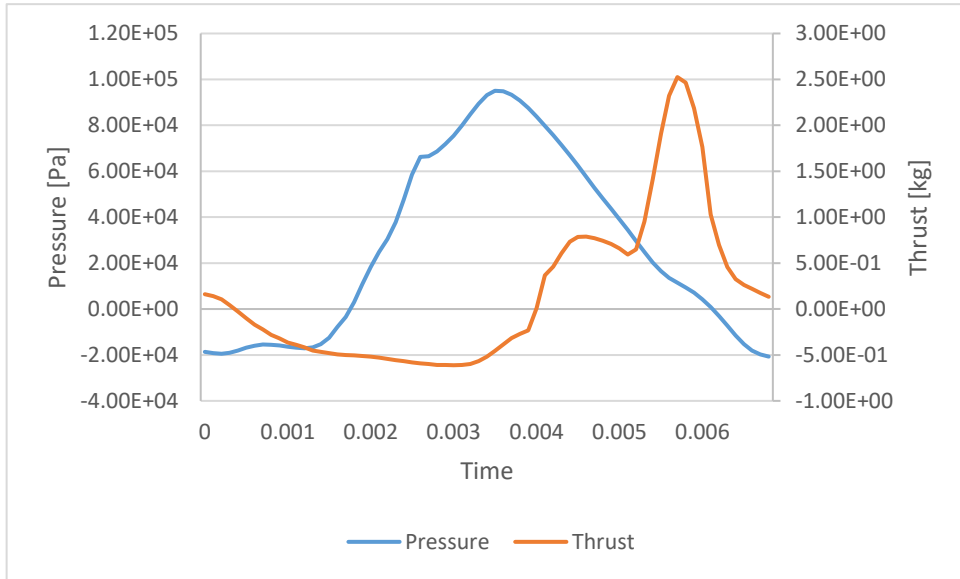


Figure 30 - Combustion chamber pressure vs thrust for case D.

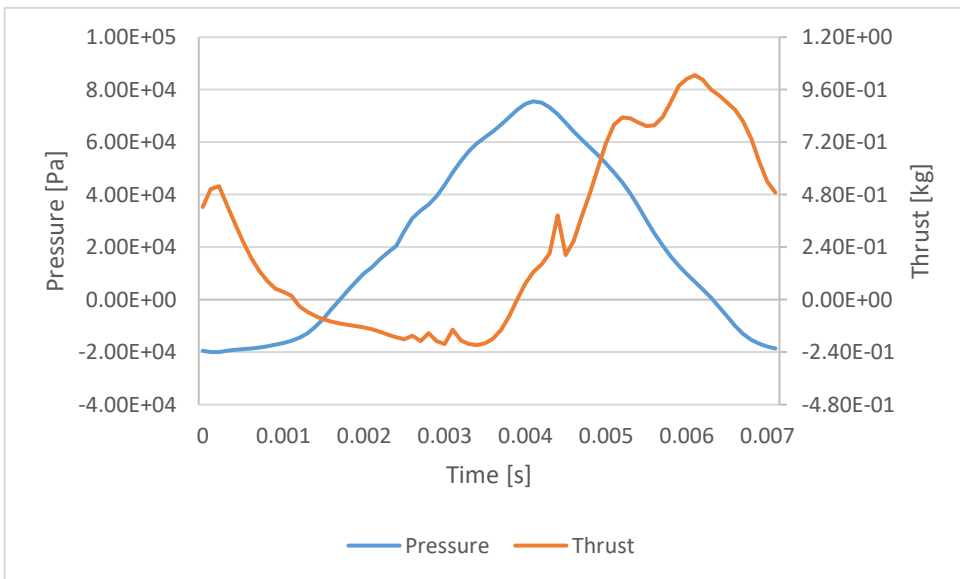


Figure 31 - Combustion chamber pressure vs thrust for case E.

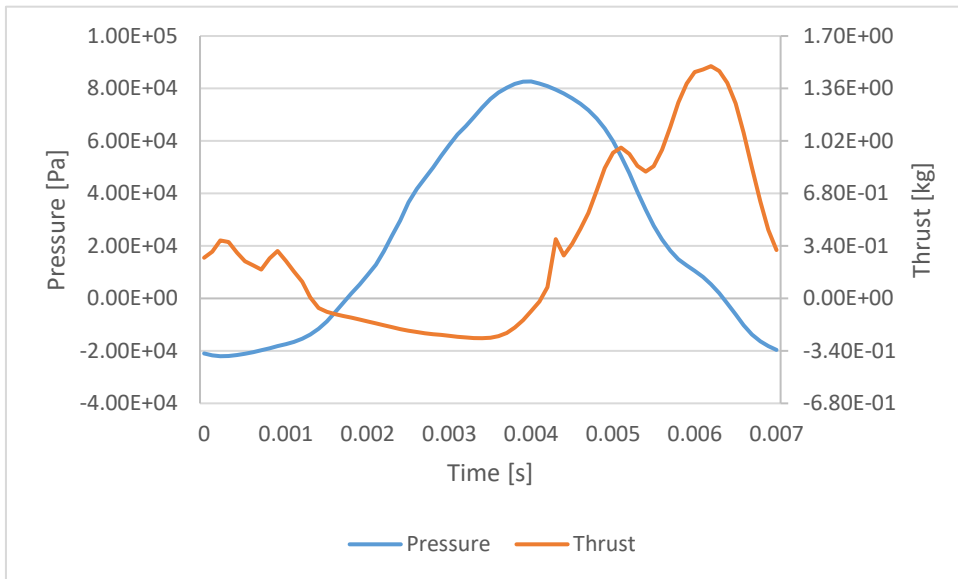


Figure 32 - Combustion chamber pressure vs thrust for case F.

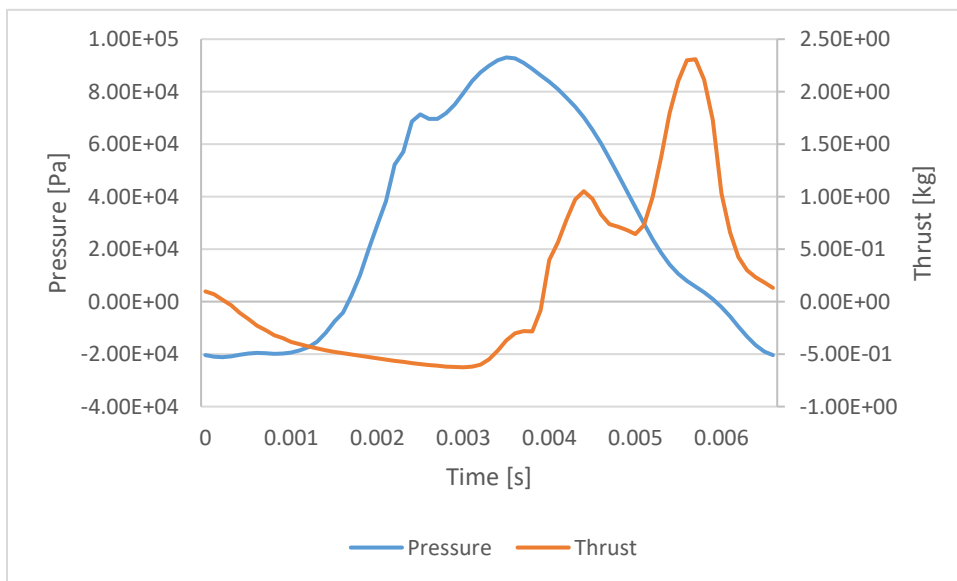


Figure 33 - Combustion chamber pressure vs thrust for case G.

5.6 Frequency

The operation frequency was compared using two different methods. The first method was using ANSYS Fluent results to observe the necessary time to complete one cycle. It was considered the beginning of the cycle when the air mass flow starts to flow into the engine through the inlet, and the end when the gases stop flowing out. For the second method, a

Matlab code was written to calculate the frequency using the model proposed by Zheng et al. [23].

The average temperature at inlet and outlet is a very important factor for the frequency calculation according to the Zheng et al. model [23]. When analysing equations 2.15 and 2.16, can be concluded that for the same engine the variable that determines the frequency is the speed of sound, and this is temperature dependent. Thus, with increasing temperature the operation frequency will increase. This is verified for both computational and calculated frequency, although being a difference between these two (see Figs. 34 and 35).

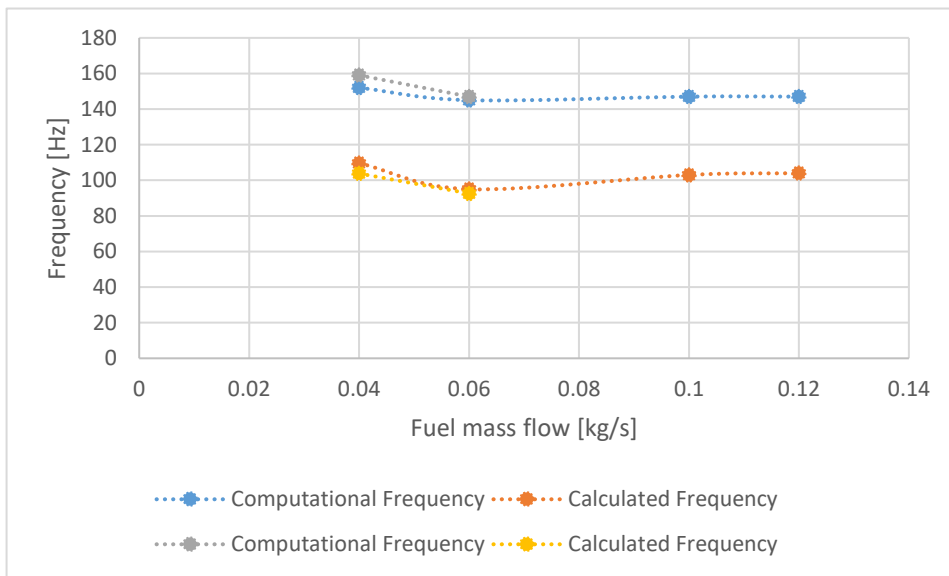


Figure 34 - Computational vs calculated frequency for propane.

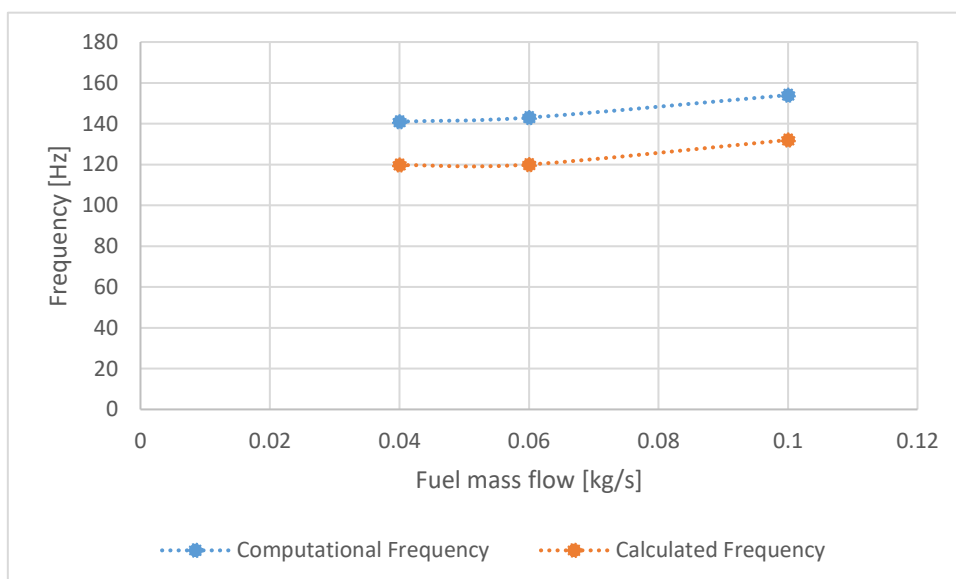


Figure 35 - Computational vs calculated frequency for methane.

For both fuels, the computational and calculated frequencies show the same behaviour. In the two first cases, for propane, the operational frequency decreases with increasing mass flow rate, while in methane, the frequency increases. For cases C and D, the computational frequency is the same, however, the calculated frequency is a little higher for case D. The results reported for methane agree with the results by Geng [10], where it was also verified that operational frequency increase with increasing fuel mass flow. The difference between the computational and the calculated frequency is higher for propane, being the largest difference around 35%.

The frequencies obtained for the two fuels are different, which goes against the results by McCalley [37]. In his study a comparison was made between kerosene and propane, and it was stated that the fuel does not influence the operational frequency. When comparing the fuels for the same conditions (case C and G), is verified that methane has a higher operating frequency.

Chapter 6

Conclusion and future work

6.1 Conclusion

A numerical study of a valveless pulsejet engine using the software ANSYS Fluent 16.2 was presented. Was aimed sizing and analysing of the performance of a valveless pulsejet for three different fuel mass flows of propane and methane as fuels.

First, taking literature in consideration, was conducted a sizing based on established principles. Given that few information was found regarding the sizing of valveless pulsejet engines, new relations were deduced in order to perform an initial sizing. After this step being completed, it was necessary to validate it, so was proceeded to the next phase: doing the computational analysis using the software previously mentioned.

Was concluded that valveless pulsejet engines are very sensitive with the fuel stream position. Initially, no pulsating effect was found. After several tests and research, was realized that for this type of engines the pulsating effect is more easily reached when the fuel is injected directly into the combustion chamber. For all the seven cases, a self-sustaining combustion was observed, and the pulsating effect was achieved.

For both fuels, the variables shown similar behaviour, however, it was verified that for propane, lower fuel mass flows lead to an inconsistent working. For methane, even with lower fuel flow, the engine showed a consistent performance.

As observed in figures 19 to 25, the exhaust temperature is higher for propane, while in methane there seems to be more excess air. For lower fuel mass flows the presence of excess air in the exhaust phase for the two fuels is evident. With increased fuel flow this excess air becomes smaller and the exhaust temperatures increases. In appendix D it is possible to observe that for methane the mass flow of air entering the engine decreases with increasing fuel flow. For propane the opposite is verified, however, the increase in air mass flow becomes less significant in relation to the increase in the fuel flow. This leads the mixtures becoming richer (higher amounts of fuel for identical amounts of air).

In what concerns the pollutant emissions, methane has better results. The formation of pollutants analysed showed substantially lower concentration. As methane has less density mixes better with air, which leads to a more efficient combustion and less formation of pollutants.

Comparing the engine performance for propane and methane under same conditions, methane showed a better performance. For the same amount of fuel, methane gives higher exhaust velocities, higher peak pressure, produced more thrust and had less formation of pollutants. Nonetheless, the behaviour of some variables is mutual to both fuels, with increasing fuel mass flow:

- The exhaust velocity at the outlet increase;
- The peak pressure in the combustion chamber increase;
- The produced thrust increase;
- The formation of CO , CO_2 and NO_x increase.

The calculated thrust is lower than the expected. The engine sizing was done based on the desire thrust of 6 kg and the maximum thrust produced was 2.5 kg. Therefore, the sizing procedure or the tested conditions did not prove to be the most completely appropriate to achieve the desire goal. Nevertheless, results are similar as the ones from similar size pulsejets.

Computational and calculated frequencies showed different values, however the behaviour is the same. Frequency decreases with decreasing fuel mass flow for case A and B the and is almost equal for case C and D. For methane, for all cases, the operational frequency increases with increasing fuel mass flow.

One of the greatest difficulties in the execution of this study was the lack of information. Despite being an engine with many years, it has been forsaken for a long time and the most recently developed studies are more focused on valved pulsejets. As already mentioned, it was difficult to obtain the pulsating combustion and find a fuel mass flow range for which the engine would get working.

6.2 Future work

Pulsejets are a very simple type of engines. Despite this, its operation is not fully understood, so, studies should continue to be carried out, especially for the valveless type. In the present study, the sizing was simplified and was not made an in-depth approach. Therefore, it is important in future works to try to optimize the performance of this engine varying its sizing and developing a calculation routine more efficiently. The computational resources are improving, and computational results are becoming more accurate. Nevertheless, it is also relevant to perform experimental studies and compare them with computational ones.

Another simplification made in the accomplishment of this project was the simulation being performed in two-dimensional. Although this type of simulation gives a good approximation of the behaviour of the flow, a turbulent flow should be performed in a three-dimensional simulation to fully capture the flow motion.

Among these main findings is that valveless pulsejet engines are very sensitive to the position of the fuel stream. Therefore, it is important to test different positions for the fuel stream inside the combustion chamber, as well as other fuels, to evaluate the changes in performance.

One of the advantages of this type of engines is the fact that not having moving parts allows the engine to work in a wide range of sizes. This makes pulsejet engines, especially valveless, very attractive to be applied in micro-propulsion systems. Future developments in this area are expected, and new findings that may minimize their size and allow achieving a good performance.

Bibliography

- [1] G. D. Roy, S. M. Frolov, A. A. Borisov and D. W. Netzer, "Pulse detonation propulsion: challenges, current status and future perspective," *Progress in Energy and Combustion Science* , pp. 545-672, 2004.
- [2] R. L. Ordon, "EXPERIMENTAL INVESTIGATIONS INTO THE OPERATIONAL PARAMETERS OF A 50 CENTIMETER CLASS PULSEJET ENGINE," Master's Thesis , North Carolina State University, 2006.
- [3] B. Ogorelec, "Valveless Pulsejet Engine 1.5 - a historical review of valveless pulsejet designs," 2005. [Online]. Available: <http://www.pulse-jets.com/valveless/>. [Accessed 27 February 2018].
- [4] Various, "Project SQUID - Final Technical Report," School of Mechanical Engineering, Indiana, 1980.
- [5] A. F. El-Sayed, *Fundamentals of Aircraft and Rocket Propulsion*, London: Springer, 2016.
- [6] B. Simpson, "The Enthusiast's Guide to Pulsejet Engines," 2004. [Online]. Available: <http://www.pulsejetbook.com>. [Accessed 27 February 2018].
- [7] R. M. Lockwood, E. L. Bennett and D. A. Graber. USA Patent US3462955A, 1969.
- [8] R. Ouellette, "Pulsejet ejector thrust augmentor". USA Patent US20050000221A1, 2002.
- [9] M. Schoen, "Experimental Investigation in 15 Centimeter Class Pulsejet Engines," Master's Thesis, North Carolina State University, 2005.
- [10] T. Geng, F. Zheng, A. Kiker, A. Kuznetsov and W. Roberts, "Experimental and numerical investigation of an 8-cm valveless pulsejet," *Experimental Thermal and Fluid Science*, pp. 641-647, 2007.
- [11] A. Kudesia and A. M. Bisen, "FUTURE ASPECTS OF VALVELESS PULSE JET," *International Journal of Advanced Technology in Engineering and Science* , vol. 3, 2015.
- [12] L. A. N. M. Lopez, D. K. S. Ting and E. Angelo, "A pulse jet operational simulation through computational fluid dynamics," in *19th International Congress of Mechanical Engineering*, Brasília, 2007.

- [13] J. Isac, L. Mohanraj, E. Sai and V. Kannan, "Numerical simulation of a hydrocarbon fuelled valveless pulsejet," *Propulsion and Power Research*, 2014.
- [14] M. Trancossi, O. Mohammedalamin, J. Páscoa and F. Rodrigues, "Thermodynamic analysis and preliminary design of the cooling system of a pulsejet for aeronautic propulsion," *International Journal of Heat and Technology*, pp. 528-534, 2016.
- [15] A. M. Rahmatike, W. Widiyastuti, S. Winardi, T. Nurtono, S. Machmudah, Kusdianto and I. M. Joni, "CFD simulation of pulse combustion's performance," *AIP Conference Proceedings*, 2016.
- [16] V. Ganesan, *Gas Turbines*, 3rd ed., New Delhi: Tata McGraw-Hill, 2010.
- [17] P. Torda, V. P. I. and B. H. J., "Compressible flow through reed valves for pulse jet engine," Technical Report No. 9, 1948.
- [18] K. A. Sai, K. Vamsi and P. S. Srinivas, "Design of Pulse Jet Engine for UAV," *International Journal of Engineering Research & Technology*, vol. 3, 2014.
- [19] C. Kerr and J. Reynolds, "Progress Report - Pulsejet Engine," San Luis Obispo, 2010.
- [20] C. E. Tharratt, "The Propulsive Duct," *Aircraft Engineering and Aerospace Technology*, vol. 37, pp. 327-337, 1965.
- [21] J. H. Lee, B. Dhar and W. Soedel, "A Mathematical Model of Low Amplitude Pulse Combustion Systems Using Helmholtz Resonator-Type Approach," *Journal of Sound and Vibration*, vol. 98, pp. 379-401, 1985.
- [22] D. Maqbool and C. P. Cadou, "Acoustic Analysis of Valveless Pulsejet Engines," *Journal of Propulsion and Power*, 2016.
- [23] F. Zheng, R. L. Ordon, T. D. Scharon, A. V. Kuznetsov and W. L. Roberts, "A New Acoustic Model for Valveless Pulsejets and Its Application to Optimization Thrust," *Journal of Engineering for Gas Turbines and Power*, vol. 130, July 2008.
- [24] B. Simpson, "How Pulsejets Work," 9 June 2001. [Online]. Available: <https://aardvark.co.nz/pjet/howtheywork.shtml>. [Accessed 9 April 2018].
- [25] J. Astrand, "Performance Prediction of a Valved and Valveless Pulse-je Engine Running on Alternative Fuel," Master's Thesis, Lulea University of Technology, 2014.
- [26] C. Hirsch, *Numerical Computation of Internal and External Flows - Fundamentals of Computational Fluid Dynamics*, 2^a ed., vol. 1, ELSEVIER, 2007.

- [27] "ANSYS Fluent Theory Guide," [Online]. Available: <http://www.pmt.usp.br/ACADEMIC/martoran/NotasModelosGrad/ANSYS%20Fluent%20Theory%20Guide%2015.pdf>.
- [28] C. D. Argyropoulos and N. C. Markatos, "Recent advances on the numerical modelling of turbulent flows," *Applied Mathematical Modelling*, pp. 693-732, 2014.
- [29] J. Fernández, "Study of Combustion Using a Computational Fluid Dynamics Software," Master's thesis, University of Barcelona, 2015.
- [30] D. Poitou, M. Hafi and B. Cuenot, "Analysis of radiation modeling for turbulent combustion: development of a methodology to couple turbulent combustion and radiative heat transfer in LES," *Journal of Heat Transfer*, 2011.
- [31] "Modeling Turbulent Flow - Introductory FLUENT Training," [Online]. Available: http://www.southampton.ac.uk/~nwb/lectures/GoodPracticeCFD/Articles/Turbulence_Notes_Fluent-v6.3.06.pdf. [Accessed 12 January 2019].
- [32] B. Nikhil, G. Purnivas, B. V. B. Rao, N. K. Chakravarthy and N. L. Prasad, "Design and Performance Analysis of Liquid Fueled Pulsejet Engine," *International Journal of Research in Engineering & Advanced Technology*, 2014.
- [33] P. R. Karteek and B. V. N. Praveen, "Design of a Advanced Focused Wave Pulsejet Engine," *International Journal of Research in Engineering & Advanced Technology*, 2014.
- [34] *ANSYS Fluent Meshing User's Guide - Release 15*, ANSYS Inc, 2013.
- [35] T. Avinash and B. Reddy, "Design and CFD Analysis of Pulse Jet Propulsion Engine," *International Journal of Professional Engineering Studies*, vol. VII, 2016.
- [36] P. J. Litke, F. R. Schauer, D. E. Paxson, R. P. Bradley and J. L. Hoke, "Assessment of the Performance of a Pulsejet and Comparison with a Pulse-Detonation Engine," in *43rd AIAA Aerospace Sciences Meeting and Exhibit*, 2005.
- [37] C. T. McCalley, "Experimental Investigation of Liquid Fueled Pulsejet Engines," Master's Thesis, North Carolina State University , 2006.

Appendix A

Pulsejet dimensions

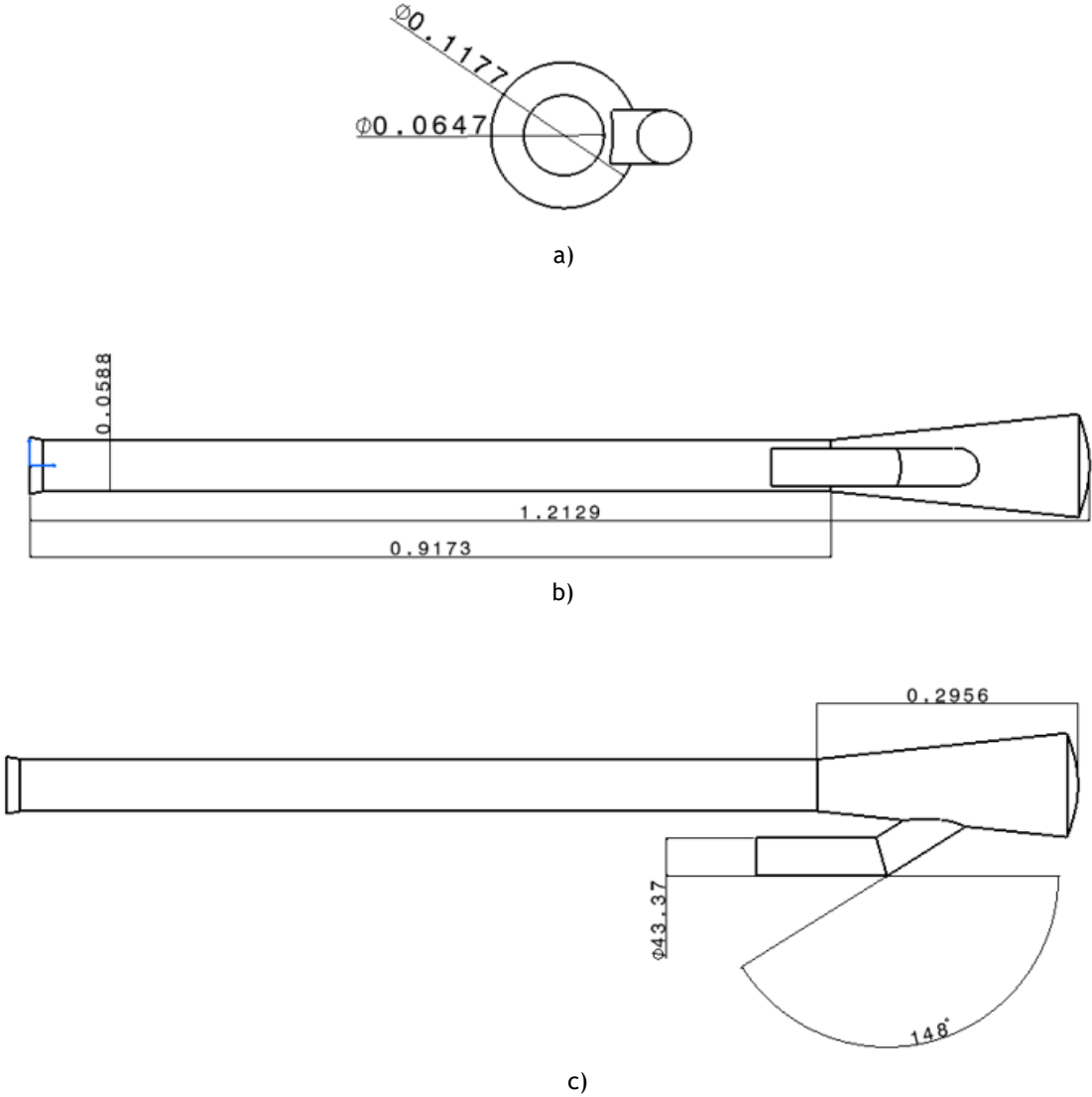
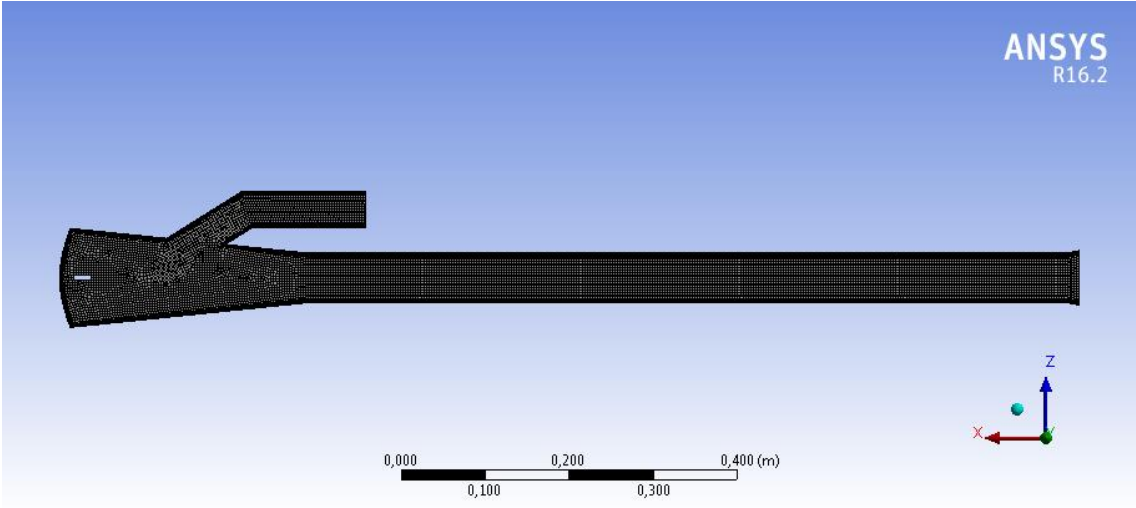


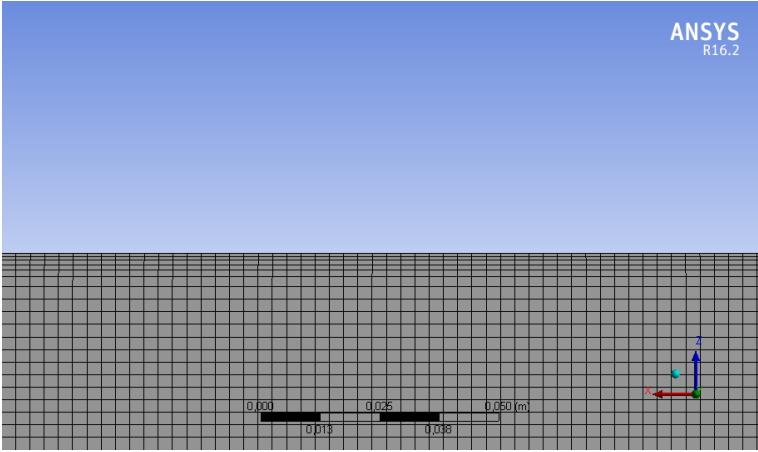
Figure 36 - Pulsejet views a) front view, b) top view and c) side view.

Appendix B

Mesh



a)



b)

Figure 37 - a) Mesh overview b) approximate view of the inflation layer

Appendix C

Matlab code

`% ansys values`

`T_in=350; %inlet temperature`

`T_ex=1500; %exhaust temperature`

`p_air=1.0135; %air pressure`

`%constants`

`gamma_air=1.4; %unburnt mixture`

`gamma_mix=4*10^(-12)*T_ex^3+4*10^(-9)*T_ex^2-8*10^(-5)*T_ex+1.3731; %burnt mixture`

`R_air=286.9; %air specific gas constant`

`R_prop=188/518; %propane/methane specific gas constant`

`A_in=0.0014775; %inlet area`

`A_ex=0.002719; %exhaust area`

`V_cc=0.0018653; %combustion chamber volume`

`L_in=0.213323; %inlet lenght`

`L_ex=0.917319; %exhaust length`

`%speed of sound`

`c_in=sqrt(gamma_air*R_air*T_in);`

`c_ex=sqrt(gamma_mix*R_prop*T_ex);`

`%Inlet frequency`

`f_in=c_in/(2*pi)*sqrt(A_in/(V_cc*L_in))`

`%Exhaust frequency`

`f_ex=[0:2000];`

`f1=@(f_ex)(tan(2*pi*f_ex*L_ex/c_ex));`

`f2=@(f_ex)((A_ex*c_ex)/(2*pi*f_ex*V_cc));`

`xstart = [50 200];`

`f_ex_sol = fzero(@(f_ex) f1(f_ex) - f2(f_ex),xstart)`

`%Total frequency`

`f_tot=(f_in+f_ex_sol)/2`

Appendix D

Air mass flow rate

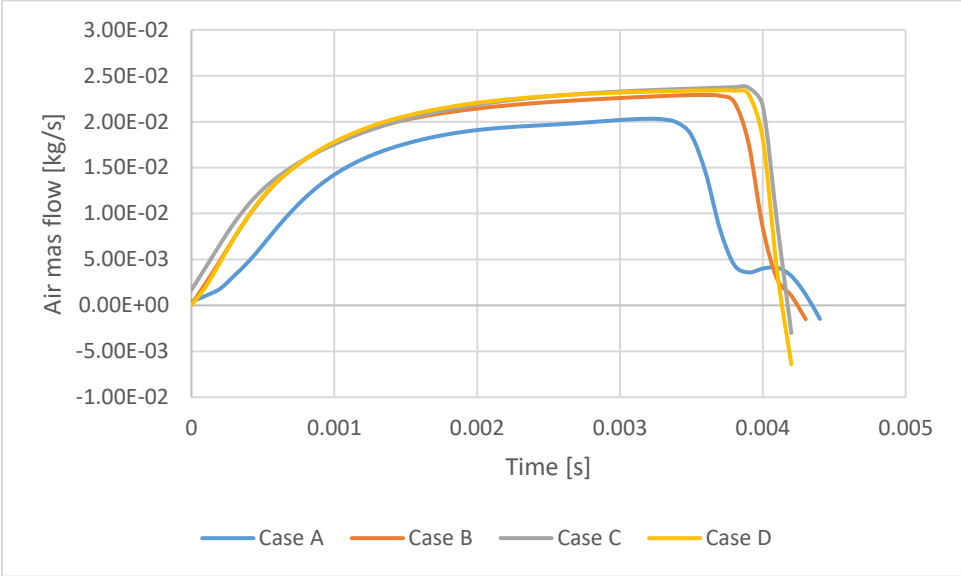


Figure 38 - Air mass flow rate for propane.

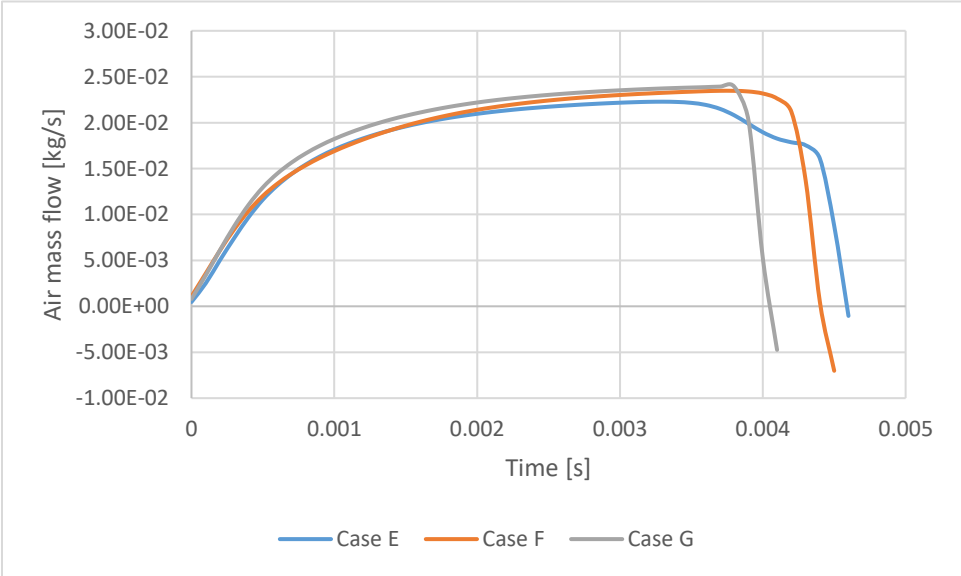


Figure 39 - Air mass flow rate for methane.